Separation and Purification Technology 419 (2026) 140303

Contents lists available at ScienceDirect

Separation and Purification Technology

journal homepage: www.elsevier.com/locate/seppur

Advancing PFAS removal and concentrate treatment: a high recovery antiscalant-free hybrid RO approach

Martin Futterlieb [a,*], Mirjana Futterlieb [a], Peter Leube [b], Avner Ronen [c], Stefan Panglisch [a,d,e,f]

[a] University of Duisburg-Essen, Lotharstr. 1, 47057 Duisburg, Germany
[b] Federal Institute for Materials Research and Testing, Division 4.4 – Thermochemical Residues Treatment and Resource Recovery, Unter den Eichen 87, 12205 Berlin, Germany
[c] Zuckerberg Institute for Water Research, The Jacob Blaustein Institutes for Desert Research, Ben-Gurion University of the Negev, Sde-Boqer 8499000, Israel
[d] IWW Water Center, Moritzstraße 26, 45476 Mülheim an der Ruhr, Germany
[e] Center for Water and Environmental Research (ZWU), Universitätsstraße 2, 45141 Essen, Germany
[f] DGMT German Society of Membrane Technology, Geschäftsstelle ZWU, Universitätsstraße 2, 45141 Essen, Germany

ARTICLE INFO

Editor name: Junyong Zhu

Keywords:
PFAS
Trifluoroacetic acid (TFA)
Closed-circuit reverse osmosis (CCRO)
Antiscalant-free desalination
Concentrate treatment
Ion exchange resins

ABSTRACT

Reverse osmosis (RO) is increasingly applied for PFAS removal from contaminated inland waters but generates a highly concentrated reject stream, complicating concentrate management. However, concentrate post-treatment may offer advantages due to reduced volumetric flow and elevated PFAS concentrations, while high-recovery operation can improve both RO economics and treatment feasibility. Nevertheless, the limited implementation of concentrate treatment leaves uncertainties, e.g., regarding the effects of elevated PFAS and competing constituents, while high-recovery operation is constrained by membrane scaling, conventionally mitigated by antiscalants, which are increasingly viewed critically. To address these challenges, two complex real water matrices with contrasting PFAS levels, both prone to $CaCO_3$ scaling and organic fouling, were investigated. Following particle removal, partial softening with weak and strong acid cation exchange resins (WAC, SAC) was evaluated as an alternative scaling control. Additionally, concentrate and raw water treatment were evaluated using PFAS-specific precipitation and powdered activated carbon. The results demonstrated that WAC offered the highest potential for scaling mitigation via synergistic hardness removal and pH reduction and employment of closed-circuit RO mitigated organic fouling and achieved exceptional recoveries up to 98.4%. The commercial membrane (BW30) maintained high PFAS rejection, including short- and ultra-short-chain compounds. Notably, concentrate treatment and higher recoveries improved specific PFAS removal while reducing chemical demand, particularly for long-chain PFAS. Conversely, for certain PFAS compounds (e.g., short-chain, carboxylic PFAS), increased recovery increased load removal but reduced removal efficiencies, likely due to competitive effects from co-occurring constituents, which may limit compliance with threshold values and highlights the need for further research.

1. Introduction

Dense membrane filtration, nanofiltration (NF) and reverse osmosis (RO), have emerged as effective options for *per*- and polyfluoroalkyl substances (PFAS) removal from contaminated water sources, with RO in particular enabling the removal of a wide range of PFAS, including short-chain and ultra-short chain species [1–5]. Compared to conventional water treatment, e.g., aeration, coagulation, flotation, river bank filtration, sand filtration, as well as advanced treatment processes, such as porous membrane filtration, ozonation, granular activated carbon and anion exchange, RO offers superior PFAS removal [1,4] and thus has been implemented in full-scale for PFAS removal for inland desalination applications [6].

One disadvantage of RO and NF operation is the generation of a concentrated waste stream (concentrate or brine) enriched in PFAS and potentially necessitating post-treatment [4,6]. However, post-treatment offers several advantages for PFAS treatment in comparison to direct treatment of the feed. The concentrate typically accounts for only about 10–25% of the raw water volume, which enables the use of more compact treatment units. Furthermore, the elevated concentrations can

* Corresponding author.
E-mail address: martin.futterlieb@uni-due.de (M. Futterlieb).

https://doi.org/10.1016/j.seppur.2026.140303
Received 20 July 2026; Received in revised form 21 September 2026; Accepted 23 September 2026
Available online 23 September 2026
1383-5866/© 2026 The Authors. Published by Elsevier B.V. This is an open access article under the CC BY license (http://creativecommons.org/licenses/by/4.0/).
Open access funding enabled and organized by Projekt DEAL.

also enhance the performance of subsequent treatment processes such as adsorption processes. Franke et al. [7] demonstrated that, when treating NF concentrate, specific PFAS removal (mass removed PFAS per volume of adsorbent) was 2.6 times higher with granular activated carbon (GAC) and 4.1 times higher with anion exchange resins compared to raw water treatment. Therefore, concentrate treatment can be more economically viable than raw water treatment [8].

Thus, the idea of increasing the RO recovery to address several challenges simultaneously is compelling. For inland desalination plants, high recoveries are a prerequisite for economically viable operation due to the difficult disposal of concentrates, limited water abstraction rights, and the need to minimize specific energy consumption (see Supplementary Information Fig. S3). Moreover, with respect to PFAS destruction, i.e., defluorination, high-temperature incineration presently constitutes the most viable option [9], and its economic feasibility improves significantly as the treatment volume is reduced, i.e., by minimizing brine through maximized recovery. This is particularly relevant for ultra-short-chain PFAS, which are essentially not retained by conventional drinking water treatment technologies [5], but occur at elevated concentrations, for instance in the European River Elbe, where they represent the primary contributor to the overall PFAS load [10].

Consequently, increasing the recovery may not only improve the overall economics of RO operation, but also open up novel opportunities for concentrate management, potentially offering more attractive treatment options compared to direct treatment of the raw water. However, attaining high recoveries also entails certain drawbacks. First, it may compromise the retention of constituents, particularly PFAS [11,12]. Second, elevated solute concentrations in brines may hinder the post-treatment of short-chain PFAS, for example by increasing competition from co-occurring ions [13] and organic matter [14]. Moreover, attaining high recoveries is constrained by membrane scaling, which in current practice is controlled through the application of antiscalants. While effective for scaling control [15], antiscalants can introduce further challenges, including their potential permeation [16,17], which may raise public health concerns and, under unfavorable conditions, contribute to the formation of harmful disinfection by-products [18]. Moreover, the detection and quantification of antiscalants is not yet established as standard analytical practice. In particular, the analysis of antiscalants in the permeate is complex and represents a considerable analytical challenge [17]. This is problematic in the context of PFAS treatment, as the use of RO to remove PFAS may be undermined if additional treatment chemicals introduce new contaminants or risks that are themselves challenging to quantify. Moreover, concentrate treatment is becoming increasingly important but may be hampered by the presence of antiscalants. For example, antiscalants can deteriorate salt removal by precipitation [19] and may compete with PFAS for adsorption sites, thereby reducing the effectiveness of PFAS removal.

Thus, this study investigates options for high-recovery RO operation to concentrate PFAS for facilitated post-treatment of the RO concentrate while producing a nearly PFAS-free permeate, without the use of scale inhibitors. To enable high-recovery operation without antiscalants, ion exchange (IEX) pre-treatment is implemented. IEX is applied in practice for scale control by removing scaling-relevant ions [20] and is subject of ongoing research into novel configurations and synergistic coupling with RO operation, particularly to reduce regeneration brines [21–24], a major barrier to wider IEX implementation [25].

First, the experimental system and methodology were characterized, including the expected PFAS rejection by the membrane system and potential adsorption of PFAS to system components (chapter 3.1.1), before assessing the influence and suitability of different ion-exchange resins used for (partial) softening as pre-treatment on the subsequent RO stage (chapter 3.1.2). Second, the influence of different pre-treatment options, operating conditions (permeate flux, recovery), and modes of operation (continuous vs. closed-circuit) on membrane performance in terms of scaling, fouling, and the rejection of standard water quality parameters and PFAS, including short und ultra-short-chain PFAS, were investigated (chapter 3.2). Third, a comparison between raw water treatment and concentrate treatment at different recovery ratios was conducted (chapter 3.4). In this context, this study addresses whether high recovery is beneficial overall, given that the concomitant concentration of salts and natural organic matter (NOM) may impair the subsequent removal of PFAS, in particular of short-chain PFAS.

The experiments were conducted at technical scale using two challenging real water matrices both prone to $CaCO_3$ scaling and organic fouling but representing high and low PFAS contamination scenarios. A hybrid treatment train was investigated, comprising conventional pre-treatment (cartridge filtration, iron and manganese removal), ultrafiltration (UF), partial softening by IEX, and a RO stage. The resulting concentrates were subsequently treated using different PFAS removal strategies, including the PFAS-specific precipitation agent PerfluorAd® [26] and powdered activated carbon.

Although previous studies have investigated advanced treatment trains for high-recovery RO operation [21,23,27], the use of CCRO to enable high recovery and PFAS removal [11,12], PFAS removal from concentrates [13,28] as well as comparing raw-water and RO-concentrate treatment for PFAS removal [7], important knowledge gaps remain regarding the interactions among individual treatment steps. It is insufficiently understood how increasing recovery affects PFAS retention, scaling and fouling propensity, and the composition and subsequent treatability of the resulting concentrate, as well as which pretreatment and operational strategies can mitigate these adverse effects.

The novelty of this study therefore lies in its holistic assessment of a treatment train for two real PFAS-contaminated water matrices with differing PFAS concentrations on a technical scale. The study evaluates IEX softening as a pretreatment strategy to enable high-recovery operation without antiscalant addition, investigates CCRO as an operational strategy to mitigate organic fouling at elevated DOC concentrations, and assesses the effects of high-recovery operation on membrane performance. Thereby providing practically relevant performance data, e.g., evaluating the retention of ultra-short-chain PFAS by commercially available RO membranes under realistic high-recovery conditions.

Finally, it compares the downstream treatment of concentrates generated at different recovery levels with direct raw-water treatment, thereby assessing whether increased recovery provides an overall benefit despite the concurrent concentration of salts and organic matter. A further novel aspect is the antiscalant-free process design. Avoiding antiscalant addition may become increasingly relevant in view of stricter regulatory requirements and growing concern regarding antiscalant use in drinking-water treatment. In addition, antiscalant-free operation may simplify subsequent concentrate treatment, for example by avoiding interference with precipitation processes or competition for adsorption sites.

2. Material and methods

2.1. Feed water

Two different real water sources were evaluated, referred to as raw water 1 and 2. Here, “raw” denotes the state of the water before any studied pre-treatment. Raw water 1 is hard groundwater from a contaminated site (aqueous film-forming foam) with a high concentration of PFAS ($\sum PFAS_{20} \approx 4,000\ ng/L$), particularly PFBA ($C_4$), PFPeA ($C_5$), PFHxA ($C_6$) and PFHxS ($C_6$). Additionally, it exhibits elevated levels of iron (approximately 0.1 mg Fe/L) and turbidity (>10 FNU). Raw water 1 was collected onsite and delivered to the lab. Raw water 2 is service water supplied from the potable water distribution system Duisburg. It is moderately hard and has low levels of PFAS. [29]. Typically, only PFBA, PFHxA, and PFOA (C_8) are detectable ($\geq$ 1 ng/L). It is in compliance with recent German drinking water regulations. Table 1 summarizes the compositions of raw water 1 and 2.

For trifluoroacetic acid (TFA), the minimum and maximum values

Table 1
Composition of raw water 1 and 2.

Parameter	Unit	Raw water 1	Raw water 2
pH	–	7.1	7.9
Conductivity	µS/cm	730	446
TDS	mg/L	530	351
Sodium		21	20.0
Potassium			5.0
Calcium		102	70.0
Magnesium		13	4.0
Chloride		16	29.0
Hydrogen-carbonate		310	165
Nitrate		3	12
Sulfate		97	46
Fe_{total}		0.1	–
Iron error	%	2.3	−4.8
Total hardness	mg/L $CaCO_3$	308	191
Carbonate hardness		254	135
TOC	mgC/L	3.15	2.68
SAC	(1/m)	7.7	7.6
SUVA	L/(mgC*m)	2.4	2.5
Turbidity	FNU	13	<0.1
$SI_{Calcite}$	(−)	−0.07	0.41
$\sum PFAS_{20}$	ng/L	≈4000	10–30
$\sum PFAS_4$		≈1000	4–12
TFA	µg/L	1.2–1.6 ($n = 2$)	1.7–4.4 ($n = 4$)

are reported, along with the number of sampling campaigns (in brackets). The distribution of PFAS in the raw water is further displayed in the Supplementary Information Fig. S1 along with additional details on PFAS sum parameters.

Raw water 1 represents a typical hard groundwater sample for remediation purposes or for drinking water treatment with multiple treatment objectives, such as iron removal, PFAS removal, and softening. Raw water 2 was selected because its quality is representative of a typical (pre-treated) feed to a dense membrane stage. On the one hand, it symbolizes the challenge of concentrating and removing low-concentration contaminants, while at the same time representing a demanding water matrix that causes both $CaCO_3$ scaling and organic fouling [30,31]. Moreover, it contains ultra-short-chain PFAS, such as TFA (1.7 to 4.4 µg/L), for which no regulatory thresholds currently exist yet [10].

2.2. Experimental procedure

Depending on the specific experiment, various water qualities were generated that differed in terms of the raw water source, the applied pre-treatment, and the chosen operating conditions. The experimental procedure is illustrated in Fig. 1 and all experiments with their respective settings are summarized in Table 2.

2.2.1. Preliminary experiments

Preliminary experiments were conducted to characterize the membrane and to evaluate the impact of IEX pre-treatment on both raw waters. All membrane tests were conducted with BW30 2540 (DuPont) [32]. The commissioning of new membranes and the cleaning process were conducted in accordance with our previous study [31]. The membrane was initially characterized in terms of its rejection performance toward standard water quality parameters and selected PFAS using raw water 2 as the feed. To emulate higher PFAS pollution levels, raw water 2 was spiked with typical short-chain (≈100 ng/L PFBA, ≈250 ng/L PFBS) and long-chain (≈ 200 ng/L PFOA, ≈500 ng/L PFOS) PFAS. The objective of the spiking experiment was to ascertain whether elevated concentrations of PFAS would result in the adsorption of PFAS onto undersaturated surfaces, thereby yielding PFAS mass losses within the system. The experiment was also designed to assess the impact of high concentration differences on the analytical determination of PFAS, with the range of differences being two orders of magnitude.

Two different types of cation IEX material were tested: weak acid cation (WAC) in the proton (Lewatit® CNP 80 WS, Lanxess) and strong acid cation (SAC) in the sodium form resin (Lewatit® S 1567, Lanxess). Batch tests were conducted to assess the impact of the two IEX materials on the composition of the respective feed water. Prior to use, the resins were rinsed with deionized (DI) water to remove potential contaminants, particularly organic matter initially leaching from fresh resins. A quantity of 12 g of each resin was added to beakers containing 250 ml of the respective feed water. The contents of the beakers were then stirred for a period of 20 min, which is approximately the EBCT of the experiments using IEX pre-treatment. The resin mass was selected to avert resin exhaustion during the course of the experiments. The stirring time was determined in advance to reach equilibrium. All tests were performed twice for both resins and both raw waters, along with corresponding controls without resin addition. Following the termination of the experiments, the pH and EC of the samples were measured. The samples were then filtered (0.45 µm) to analyze ions and measure total organic carbon (TOC) and total carbon (TC) for total inorganic carbon (TIC) determination.

2.2.2. Hybrid treatment schemes

Due to the high fouling potential (elevated turbidity and iron concentrations), raw water 1 was pre-treated step wise, see Fig. 1 c). First a cartridge filter (10 µm) separated particles, which reduced the turbidity by roughly 50%. Thereafter the water was aerated and treated with an UF plant (SIMA-tec GmbH) equipped with an inside-out Multibore (DuPont) UF membrane (length 1.15 m, and 3.3 m^3 membrane surface), for advanced particle and iron removal. This resulted in turbidity of less than 0.3 FNU and a total iron concentration below 0.02 mg/L. The aeration boosted CO_2 degassing, causing the pH to rise from 7 to 8.7, which in turn led to precipitation of $CaCO_3$. The visible precipitates were retained by UF filtration.

The UF filtrate was conditioned to approximately pH 7 by adding CO_2 and was subsequently used as the RO feed in experiment 1.1 (see Table 2). For experiment 1.2 the UF filtrate was further pre-treated by partial softening using SAC-IEX. In both experiment 1.1 and 1.2, the water was completely recirculated (recirculation of permeate and concentrate back to the feed tank). The release of CO_2 associated with the full recirculation was offset by controlling the pH through CO_2 dosing.

In contrast, raw water 2 was treated continuously, i.e., the feed tank was constantly refilled with fresh raw water, while permeate and concentrate were discharged. In the experimental series 2 (Exp. 2.1 to 2.6), only partial softening by SAC- and WAC-IEX was used as pre-treatment. The same IEX columns and RO system were used for both waters for partial softening (see Fig. 1 d). Three IEX columns were operated in series (≈ 10 L of resin).

The fully automated RO pilot plant was supplied by SIMA-tec GmbH (Schwalmtal, Germany). The apparatus consists of a standard pressure vessel with a diameter of 2.5 in. and a length of 40 in., equipped with a single spiral-wound element (active membrane area 2.6 m^2). Online measurements encompass pressure (feed, concentrate, permeate), flow rate (permeate, concentrate), electrical conductivity (EC) in permeate and concentrate, pH (permeate and concentrate), and temperature. The modes of operation of the plant include continuous feed and bleed mode, which is referred to as continuous flow (coFRO), and discontinuous semi-batch, closed-circuit reverse osmosis (CCRO). Further information is available in the supplement (chapter 1.2) and our preceding studies [30,31].

2.2.3. Concentrate treatment

PFAS removal was investigated from raw water and concentrate samples to evaluate if concentrate treatment offers advantages over raw water treatment and to investigate the influence of the recovery.

In Exp. 3.1, the PFAS-specific precipitant PerfluorAd® (Cornelsen Umwelttechnologie GmbH, CU) was tested. PerfluorAd® was applied to

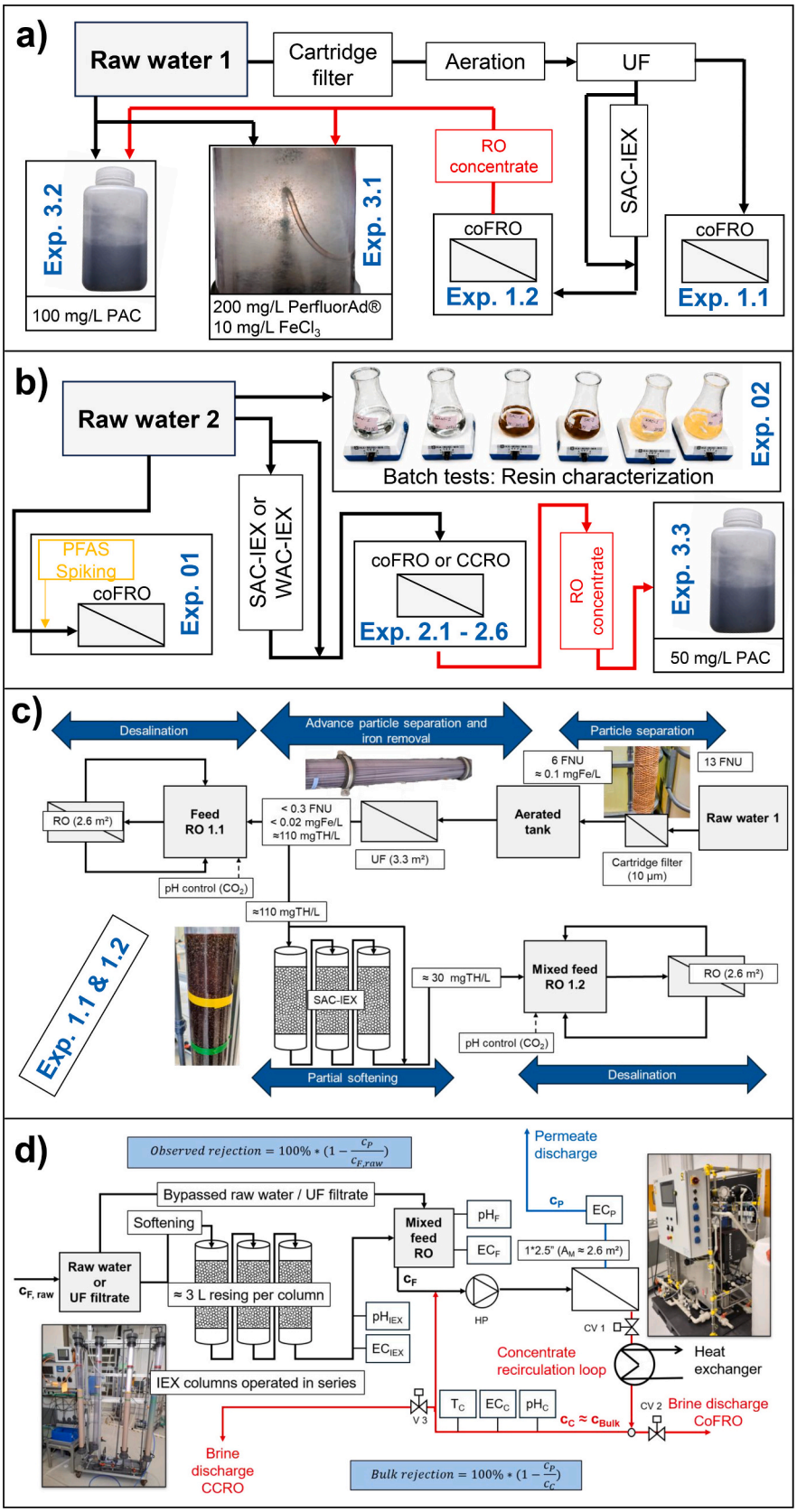


Fig. 1. Overview of different experiments for raw water 1 (a) and 2 (b); c) Detailed treatment train of raw water 1; d) Simplified P&ID and photographs of the ion exchange (IEX) columns on the left bottom corner and the membrane plant (right top corner) used for all experiments.

Table 2
Summary of experiments.

Exp. ID	Raw water (RW) type and pre-treatment	Type of experiment	PFAS-20 samples	TFA samples
0.1	RW 2 spiked with PFAS	coFRO at 25 LMH and $\phi = 80\%$	X	
0.2	RW 1 and 2	Batch tests with SAC and WAC resin		
1.1	RO feed 1.1: RW 1 after: CF, aeration + UF	coFRO at 10 LMH at 50,76 and 87% ϕ	X	
1.2	RO feed 1.2: RW 1 after: CF, aeration + UF + 80% SAC	coFRO at 10, 20 LMH at 76, 84 and 90% ϕ	X	X
2.1	RO feed 2.1: RW 2 with 50% SAC	coFRO at 20 LMH at 90% ϕ		
2.2	RO feed 2.2: RW 2 with 50% WAC	coFRO at 20 LMH at 90, 95 and 80% ϕ	X	X
2.3	RO feed 2.2: RW 2 with 50% WAC	CCRO at 20 LMH at 90% ϕ_{CC}		
2.4	RO feed 2.2: RW 2 with 50% WAC	CCRO at 20 LMH at 95% ϕ_{CC}	X	
2.5	RO feed 2.2: RW 2 with 50–70% WAC	coFRO at 15, 28.7 LMH at 96, 97.7% ϕ	X	X
2.6	RO feed 2.2: RW 2 with 40–70% WAC	CCRO at 15, 30 LMH at 97.7, 98.4% ϕ_{CC}		
3.1	RW 1 and concentrate Exp. 1.2	Precipitation: 200 mg/L PerFluorAd® + 10 mg/L $FeCl_3$	X	
3.2	RW 1 and concentrate Exp. 1.2	PAC adsorption: 100 mg/L PAC	X	
3.3	Various concentrates generated from RW2	PAC adsorption: 50 mg/L PAC	X	

raw water 1 and to the concentrates derived from raw water 1. According to the supplier's recommendation (CU), a PerfluorAd® dose of 200 mg/L and 10 mg/L $FeCl_3$ was used.

Furthermore, powdered activated carbon (PAC) was tested to study the adsorption of PFAS. PAC adsorption tests were conducted with raw water 1 and two concentrates generated from raw water 1, collected at 75% and 90% recovery. It should be noted that pre-treatment and scaling events influenced the PFAS concentration of raw water 1 (see chapter 3.2), therefore, the concentration factor related to the initial PFAS concentration (3 and 6) is significantly lower than the hydraulic concentration factor (4 and 10). Only concentrated samples of raw water 2 were used for adsorption tests because the PFAS concentration in the raw water was too low. Four different recoveries were investigated (83, 91, 96 and 98%). The concentration of PAC was set to cover the wide range of concentration factors and was fixed at 100 mg/L for raw water 1 and 50 mg/L for raw water 2. The reaction time was 72 h. Norit® SA Super (Cabot) powdered activated carbon (PAC), produced from plant-based raw materials, was used (iodine number: 1050 mg/g; median particle size $d_{50} = 15$ µm).

It is important to emphasize that the PAC tests were not primarily conducted to assess PAC treatment. Rather, their primary objective was to investigate how different feed concentration, ranging from raw water to highly concentrated streams, affect the loading capacity. Accordingly, these results can be applied to fixed-bed GAC systems, where the determination of adsorption isotherms using PAC is standard practice for initial capacity evaluation.

2.2.4. Summary of experiments

Table 2 summarizes the experiments conducted.

2.3. Analysis

Relevant cations and anions were analyzed by ion chromatography (IC) using two Metrohm Eco IC systems. The TOC and total carbon (TC) concentrations were measured using a Shimadzu TOC-L analyzer, and the total inorganic carbon (TIC) concentration was determined as the difference between the TC and TOC concentrations. Dissolved organic carbon (DOC) was determined from 0.45 µm-filtered samples using a TOC-L analyzer. The distribution of TIC species (CO_2, HCO_3^-, and CO_3^{2-}) was determined based on the measured pH. The spectral absorption coefficient (SAC) at 254 nm was determined for samples filtered through 0.45 µm membranes. Furthermore, pH and electrical conductivity (EC) were measured using WTW 3310 and inoLab Cond 7310 (Xylem Inc.) handheld devices, in conjunction with online monitoring. Further insight into lab analysis and online monitoring can be found in our previous study [31].

The analysis of PFAS was conducted in a certified commercial laboratory (IWW Analytik und Service GmbH, Mülheim, Germany) in accordance with the German Drinking Water Directive. The limit of quantification (LOQ) for PFAS from the $\sum PFAS_{20}$ list compounds is 1 ng/L.

In addition, TFA analysis was conducted using a gas chromatography – mass spectrometry (GC–MS) headspace approach [33] with an LOQ of approx. 0.5 µg/L. In brief, TFA in the water sample was automatically esterified at 80 °C with methanol and sulfuric acid in a head space vial. The formed volatile TFA-methyl ester were collected in the gas phase above the liquid phase and afterwards directly injected into a GC–MS system (GC–MS-QP2010 Ultra, Shimadzu Instruments, Japan) for analysis.

PFAS analysis is susceptible to numerous potential error sources, particularly during routine laboratory sample preparation steps such as sample filtration [34,35], as applied in this study for concentrates, PAC solutions, and PerfluorAd® samples. Prior to PFAS sample preparation, the pressure filtration system was rinsed with Milli-Q water and equipped with a new 0.45 µm filter. Filtration was then performed with the respective water matrix to pre-condition the system, and the initial filtrate, where potential adsorption or leaching effects may occur, was discarded and not used for PFAS analysis. Pre-rinsed HDPE bottles were used for sample storage and adsorption tests, pre-rinsed PP bottles for shipment, and cellulose-based filters were employed, as these materials are recommended for PFAS analysis [34].

2.4. Calculations

Permeabilities are reported as corrected permeabilities (P_c) see eq. (1), calculated as the ratio of permeate flux (J_P) to the effective driving force, i.e., the difference between transmembrane pressure (TMP) and transmembrane osmotic pressure ($TM\pi$) while accounting for temperature effects via membrane-specific temperature correction functions ($TCF_{25°C}$) provided by the membrane supplier [20]. The impact of osmotic pressure was approximated correlating (x) the electrical conductivity of the concentrate (EC_C) to the osmotic pressure.

$$P_c = \frac{J_P * TCF_{25°C}}{TMP - TM\pi} \approx \frac{J_P * TCF_{25°C}}{TMP - x * EC_C} \quad (1)$$

The recovery (ϕ) in coFRO is the fraction of permeate to discharged brine flow. For raw water 2, CCRO operation was investigated, too. In this case, the closed-circuit recovery (ϕ_{CC}) was applied, which excludes the influence of flushing and can be calculated from the system volume, the closed-circuit time, and the flux [30].

In this study, two different types of rejection were calculated, each using a different reference concentration. In Fig. 1 d), a synopsis of the various rejection calculations is provided (illustrated by the blue boxes), along with a demonstration of the distinct applied feed concentrations. Given the low single-pass recovery rate (4 to 8%), it can be deduced that the bulk and concentrate concentrations are approximately equal, see supplement Table S1. Therefore, the bulk rejection is related in an approximation to the concentrate concentration (c_C):

$$Bulk\ Rejection = 100\%^{*}\left(1-\frac{c_P}{\frac{1}{2}^{*}(c_F+c_C)}\right) \approx 100\%^{*}\left(1-\frac{c_P}{c_C}\right) \quad (2)$$

Bulk rejection was used for most results because it is (nearly) independent of recovery and therefore allows meaningful comparison with other systems, for example by practitioners. Further information on the calculation and assumptions can be found in the supplementary chapter 1.2. In addition, the bulk log removal value (LRV_{Bulk}) was calculated with:

$$LRV_{Bulk} = -log_{10}\left(c_C/c_P\right) \quad (3)$$

Moreover, the observed (plant) rejection was calculated by relating the permeate (c_P) to the feed concentration ($c_{F,raw}$) before pre-treatment, particularly to enable comparison of different pre-treatment options.

Since PFAS concentrations in most permeate samples were below the LOQ, two approaches were used to estimate rejection and permeate quality. First, a minimum rejection was calculated by assuming the permeate concentration to be equal to the LOQ (Fig. 2 f). For TFA, the permeate concentration was estimated via a mass balance based on the corresponding volumetric flow rates (Q) and concentrations (c), and was subsequently used to calculate TFA rejection:

$$c_P = \frac{Q_F{}^{*}c_F - Q_c{}^{*}c_C}{Q_P} \quad (4)$$

The saturation index (SI) and the ion balance error were calculated using PhreeqC (version 3.8.6.17100; database phreeqc.dat). In Figs. 3 and 5 also show the estimated calcite SI, representing the SI directly before the scaling event, as estimated from online EC and pH measurements. Calculations of measurement uncertainty are described in the Supplementary Information (chapter 1.3).

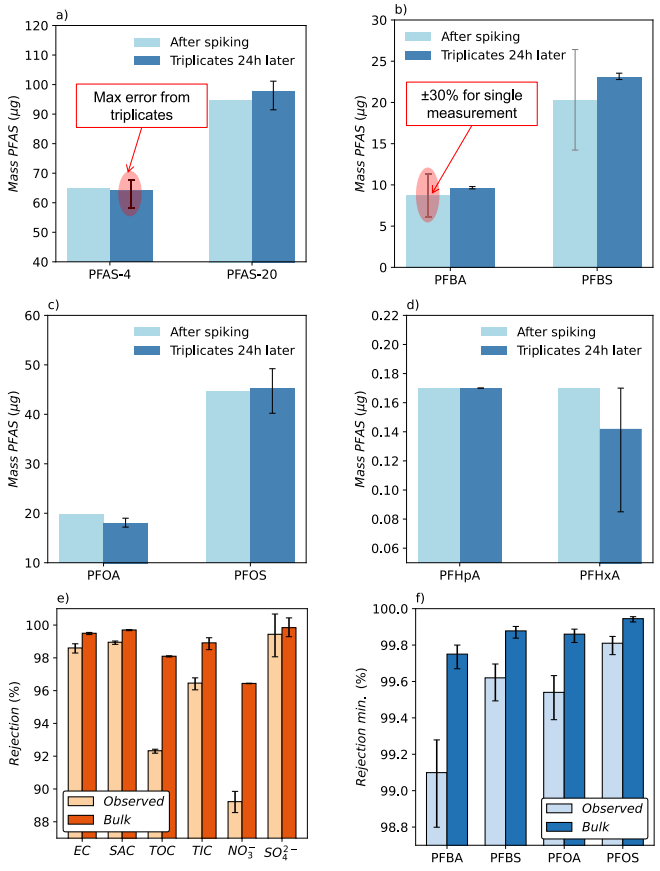


Fig. 2. Exp. 01: raw water 2 spiked with PFBA, PFBS, PFOA and PFOS. a) to d): PFAS mass in system with fully recirculated permeate and concentrate; e) Rejection at 25 LMH and 70% recovery for EC, SAC, TOC, TIC, nitrate and sulfate. f) Minimum rejection of spiked PFAS.

3. Results and discussion

3.1. Preliminary experiments

3.1.1. System characterization: PFAS losses and rejection

Fig. 2 depicts Exp. 01, in which raw water 2 was spiked with PFAS. In parts a) through d), the PFAS mass within the system is shown for PFAS sum parameter (a) the spiked PFAS compounds (b, c) and unspiked PFAS compounds (d). The left bars represent the PFAS mass immediately after spiking, whereas the right bars show the results of triplicate measurements after 24 h of filtration at a flux of 25 LMH under fully recirculated conditions, i.e., with both permeate and concentrate returned to the feed tank. For the PFAS sum parameters, PFOA, PFOS, PFHpA, and PFHxA, the differences between the PFAS masses measured immediately after spiking and after 24 h of filtration were within the variability of the triplicate measurements. The results were therefore considered consistent with the absence of relevant systematic PFAS losses. Interestingly, PFBA and PFBS showed higher measured masses after 24 h of operation. Potential explanations include contamination or artefacts during sample preparation, for example from glassware or filter materials. However, the apparent increases may also be explained by the uncertainty associated with the individual initial measurement. The differences between the left and right bars were approximately 10%, which is within the typical uncertainty range assumed for individual measurements (±30%; see the Supplementary Information chapter 1.3).

This indicates that adsorption of PFAS onto surfaces, e.g., the membrane, is not relevant for the given setup, even under high concentrations, as e.g., experienced in later experiments at high recovery and concentrate recirculation.

This is different from what has been reported about PFAS adsorption on membranes. For instance, Cao et al. [13] reported for comparable membranes an adsorption of roughly 2 $\mu mol_{PFOS}/m^2_{Membrane}$, which would translate for our system into approximately 2.6 mg PFOS adsorption. The absence of observed adsorption in our study is presumably attributable to the long service time of the system used treating real water matrices with elevated PFAS concentrations. It's likely that most of the adsorption happened earlier, and the system is nearly saturated.

The minimum rejection of PFAS (Fig. 2 f), indicated by non-detectable concentrations in the permeate, is high and consistent with reports in the literature for the same membrane [2]. Notably, minimum PFAS rejection even exceeded that of standard water quality parameters (Fig. 2 e) that are typically known to show high retention in RO, such as sulfate.

3.1.2. IEX resin batch tests

Table 3 summarizes the results of the batch tests (Exp. 02) conducted to characterize the influence of the SAC and WAC resins to raw water 2. The cation removal achieved with the SAC is substantially higher; for example, calcium and magnesium removals are 97% and 95%, respectively, compared to 78% and 63% with the WAC. This behavior is inherent to the different IEX resins: while SAC resins remove both temporary and permanent hardness nearly completely, hardness removal by a WAC resin in the hydrogen form is limited to the carbonate (temporary) hardness, i.e., the fraction associated with alkalinity [20]. In other words, exchange proceeds only as long as carbonate and bicarbonate species can buffer the released protons, and thus sufficient alkalinity is available. However, overall TDS removal is significantly enhanced by WAC, as proton release lowers the pH and shifts the dominant TIC species from bicarbonate to uncharged dissolved carbon dioxide (CO_2). This pH-induced speciation shift raises the dissolved CO_2 concentration to roughly 50 times atmospheric equilibrium, thereby

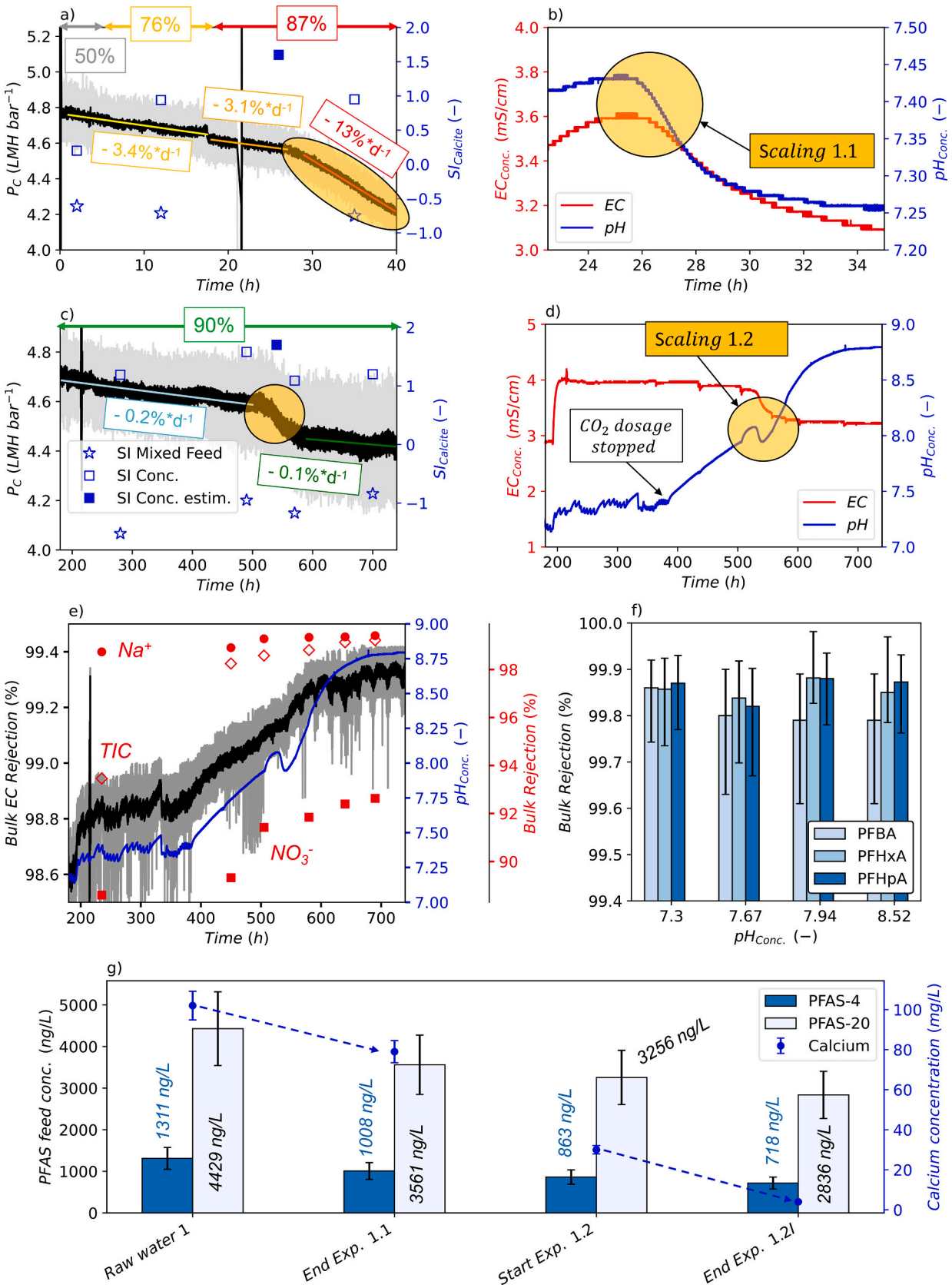


Fig. 3. Permeability, $SI_{Calcite}$, concentrate EC and pH of experiment 1.1 (a, b) and 1.2 (c, d) over time with marked scaling event; e) Rejection of: EC-, Nitrate (NO_3^-), TIC, Sodium (Na^+); and concentrate pH; f) PFBA, PFHxA and PFHpa rejection; g) PFAS and calcium feed concentrations.

Table 3
Exp. 02: Comparison of the effect of IEX pre-treatment on the properties of raw water 2. Average values from duplicate experiments with the maximum deviation indicated.

Parameter	Unit	Raw water 2	IEX-effluent	
			SAC	WAC
TDS	mg/L	350.4 ± 6.2	361.3 ± 6.7	128.8 ± 2.3
Calcium		67.9 ± 3.4	2.7 ± 0.1	14.7 ± 0.7
Magnesium		4.4 ± 0.3	0.2 ± 0.05	1.64 ± 0.06
Sodium		21.0 ± 0.7	107.9 ± 1.3	21.2 ± 0.2
TIC	mgC/L	32.9 ± 1.8	32.5 ± 1.5	8.2 ± 5.6
Bicarbonate	mg/L	161.8	161.0	0.09
Carbon dioxide		3.5	2.3	30.1
EC	µS/cm	449	451.5 ± 2	301 ± 1.4
pH		7.85 ± 0.05	8 ± 0.03	3.62 ± 0.01
SI		0.34	−0.85	−8.64
π	mbar	193	244	94
Ion-error	%	−4.8	−3.8	−3.18

driving extensive CO_2 stripping and resulting in an overall TIC removal of approximately 75%. However, it should be noted that stirring and the relatively high surface to volume ratio of the used Erlenmeyer Flasks in the batch tests favor CO_2 degassing compared to typical used feed tanks in full scale applications. Though, the high CO_2 access will still yield in TIC removal, as observed in the technical scale operation of WAC as pre-treatment for RO operation. Here, even partial softening with WAC (chapter 3.2.2), followed by blending 50% WAC-treated water with 50% untreated raw water 2, resulted in TIC removal of approximately 25–30%. Moreover, it should be emphasized that, even if less TIC were removed by CO_2 degassing at larger scale, this would not compromise the advantages of WAC operation. Reduced CO_2 removal would result in a lower pH and, consequently, in a comparable or a lower SI (depending on the extent of CO_2 degassing).

Compared to the SAC-, the WAC-IEX offers several advantages when treating water that causes $CaCO_3$ scaling. First, for WAC, the concurrent removal of calcium and bicarbonate significantly reduces the SI of calcite, whereas SAC primarily removes calcium while leaving alkalinity (almost) unaffected, which leads to factor 10 times lower SI for the WAC. Furthermore, the high TDS removal of the WAC, during (partial) hardness removal and the shifting of TIC fractions to CO_2, results in a significant reduction in osmotic pressure (π), approximately half of that of the raw water. On the contrary, the osmotic pressure after SAC treatment increases compared to the raw water. This can be explained by the ion-exchange mechanism, which releases two moles of sodium into the solution for each mole of total hardness removed [25]. In the present case, this stoichiometry increases the molar concentration of dissolved ions by roughly 2 mM, corresponding to an osmotic pressure rise of about 50 mbar.

The slight pH increase observed after SAC treatment can be attributed to changes in carbonate speciation associated with the removal of total hardness. As calcium and magnesium are removed, their aqueous carbonate complexes (such as $CaCO_{3(aq)}$ and $CaHCO_3^+$ [36]) decrease, so that a larger fraction of TIC remains as free bicarbonate and carbonate species, which leads to a modest increase in pH.

In the following, the influence of IEX pre-treatment is further investigated on a technical scale (chapter 3.2.1 and 3.2.2). Moreover, in chapter 3.2.3 both pre-treatment options are holistically evaluated.

3.2. Hybrid treatment of raw water 1

3.2.1. Raw water 1

Fig. 3 a) shows the permeability and calcite saturation of Exp. 1.1. The increase in recovery had a marginal effect on the permeability loss, which was about 3% per day for 50, 76 and 87% recovery, indicating a high fouling rate for all investigate recoveries. The high permeability decline is presumably related to organic fouling and discussed later. However, after approximately 10 h of operation at 87% recovery, a significant decline (13% per day) in permeability was observed. This decline is attributable to $CaCO_3$ scaling, as demonstrated by the characteristic decrease in the concentrate's pH and a slightly delayed concentrate EC drop [30,31], see Fig. 3 b). The drop in pH during $CaCO_3$ precipitation in scaling event 1.1 is caused by the release of protons when bicarbonate is converted to carbonate upon binding with calcium [31,37].

Following scaling event 1.1, the membrane was chemically cleaned and restored before Exp. 1.2 began, in which the feed was switched to UF filtrate that had previously been pre-treated by partial softening with SAC-IEX. In this experiment, the system was operated at 90% recovery and only a marginal decline in permeability due to fouling was observed from 200 to 500 h of operation, see Fig. 3 c). The main difference between Exp. 1.1 and 1.2 is the much lower calcium concentration (30 mg/L instead of 100 mg/L) due to SAC-IEX softening. It is therefore likely that the markedly improved permeability performance is primarily linked to the lower calcium concentration. Calcium can enhance organic fouling by promoting the formation of cross-linked gel layers with natural organic matter (e.g., alginates and humic acids), which are known to cause severe organic fouling [38,39]. Thus, for feed water with a high organic fouling potential such as raw water 1, SAC-IEX offer additional benefit compared to WAC-IEX even though its effect on $CaCO_3$ scaling prevention is less pronounced (see chapter 3.1.2 and the following chapter 3.2.2).

After approximately 400 h of operation, pH control via CO_2 dosing was stopped to investigate the effect of the higher pH on scaling formation (Fig. 3 d) and on the retention of selected standard parameters and PFAS (Fig. 3 e and f). Subsequently, a significant decrease in pH was observed at a pH of approximately 8, indicating a renewed $CaCO_3$ precipitation (scaling event 1.2). Since the concentrate and permeate were fully recirculated in Experiment 1.2, calcium accumulated on the membrane due to precipitation and thus depleted in the recirculate as the experiment progressed (<5 mg Ca^{2+}/L). Consequently, a state of equilibrium was reached after a short period, and the permeability stabilized. The pH continued to rise due to CO_2 degassing until it, too, reached equilibrium at approximately 8.8 (Fig. 3 c and d).

This highlights the strong influence of pH on $CaCO_3$ scaling: when CO_2 dosing is stopped, the saturation index rises sharply from 1.19 at pH 7.45 to more than 1.7 at pH 8 (Fig. 3 c), thereby promoting scaling at this pH. This demonstrates once more the advantage of proton exchange during softening with WAC compared to SAC.

The trend in bulk EC rejection closely follows that of the concentrate's pH value (Fig. 3 e), that is, as the pH value increases, an increase in EC rejection can be observed [30]. The increase in pH exhibited a substantial impact on the rejection of TIC, which rose from 93.5% at a concentrate pH of 7.4 to more than 99.2% at a pH of 8.8. This can be explained by the shift of TIC species toward charged components as the pH increases, meaning that the amount of uncharged CO_2, which is not retained by dense membranes [40].

Concurrently, the concentrations of the well rejected bicarbonate and carbonate and thus the TIC rejection increase with increasing pH [30]. Since bicarbonate is the dominant anion in the feed, the increase of EC rejection is largely associated with increasing TIC rejection. In addition, as the negative charge of the membrane increases with pH [2,41], the electrostatic repulsion of negatively charged compounds also increases. This, in turn, further enhances TIC rejection by increasing the rejection of bicarbonate and carbonate and also improves the rejection in general of other ions, not only anions but also cations, because the permeate must remain charge neutral [42], as exemplified by the increasing rejection of sodium and nitrate.

In contrast, PFAS rejection was not significantly impacted by the pH, see Fig. 3 f). This can be attributed to the primary exclusion mechanism of PFAS in RO membranes, namely size exclusion, rather than electrostatic interaction, which are more relevant for NF membranes [2]. Although for PFBA a higher rejection at the lowest pH was observed, this

may not be related to the pH, but to the fact that the rejection was determined before the scaling event and thus at higher calcium concentrations. Liu et al. [39] investigated the influence of the calcium concentration on PFAS rejection and found that calcium, humic substances and PFAS may bridge to larger complexes, which boost PFAS rejection, in particular rejection of short-chain PFAS, such as PFBA. Interestingly, after the second scaling event, both the decline in permeability decreased and PFBA rejection fell slightly, which might be related to a less pronounced organic fouling layer, due to the exhaustion of calcium.

Lastly, during Exp. 1.1 and 1.2, a decline of the PFAS feed concentration was observed. The concentration of PFAS-4 and PFAS-20 decreased from the raw water to the feed concentration by approximately 50% and 40%, respectively, see Fig. 3 g). Interestingly, the calcium concentration exhibited a similar decreasing trend. Moreover, after the second scaling event, the PFAS feed concentration remained constant with no further declining trend (see Supplementary Information Fig. S4). Therefore, the observed PFAS removal might be linked to $CaCO_3$ precipitation, as adsorption of PFAS onto system components had previously been ruled out, see chapter 3.1.1. $CaCO_3$ precipitation occurred during the two scaling events, in addition to aeration of the raw water for the purpose of iron removal, see chapter 2.2.2. Retention of PFAS on minerals, such as limestone ($CaCO_3$) [43] and dolomite [44] has been reported. As stated by Lv et al. [43], PFAS retention on limestone is governed by two main factors. First, electrostatic interactions: the zeta potential of limestone is generally only slightly negative and shifts toward more positive values at higher ionic strengths [43] (e.g., as given within the concentrate of our study) which enhances electrostatic attraction with negatively charged PFAS. Second, the relatively high specific surface area of limestone provides a greater density of sorption sites [43]. This may point to beneficial synergistic effects of softening processes, for example fluidized bed pellet softening, which may enable partial PFAS removal as well. The influence of $CaCO_3$ precipitation on PFAS removal was not an objective of this study. Nevertheless, the observed association appears substantial and warrants further investigation. At this stage, the proposed relationship between PFAS removal and $CaCO_3$ precipitation remains observational, as it is based solely on correlations between their concentrations. Future work should therefore systematically investigate the underlying mechanisms, for example through adsorption-isotherm experiments and by characterizing scaling layers.

Fig. 4 shows the influence of the flux on the rejection of standard parameters (a), PFAS (b) and permeability (c). As expected, the rejection of all solutes increases because solute flux remains nearly constant, while the water flux rises with increasing pressure, i.e. with increasing permeate flux, which effectively dilutes the solute concentration in the permeate [45]. Noteworthy is the sharp increase in nitrate rejection, which has risen from 92 to 96%. The in general low ion rejection is discussed later (chapter 3.2.2).

The influence of flux on PFAS rejection is particularly pronounced for ultra-short chain TFA and short-chain PFBA. The observed increase is critical for compliance with current German drinking water standards: at 10 LMH the permeate does not meet the limit, whereas at 20 LMH compliance is achieved (see Supplementary Information Fig. S5). However, the benefit of higher overall rejection at higher fluxes comes at the price of increased permeability loss, in addition to higher operating costs due to elevated pressure. Fig. 3 c) shows that the permeability decreases directly with increasing flux, which is presumably related to enhanced concentration polarization at higher flux. Moreover, the permeability decline over time increases by approximately a factor of five, which is likely associated with increased organic fouling, as discussed previously.

3.2.2. Raw water 2

Fig. 5 compares Exp. 2.1 and 2.2: operation with SAC-IEX (a, b) and WAC-IEX (c, d) as pre-treatment strategies. In both cases, 50% of the raw water was subjected to softening, while the remaining 50% bypassed treatment and was directed to the mixed feed tank. With SAC-IEX pre-treatment, permeability decreased sharply from the start (Fig. 5 a), and scaling was already indicated by a drop in concentrate pH after 3 h (Fig. 5 b). On the contrary, WAC-IEX pre-treatment enabled stable operation with moderate permeability drop at recoveries of 90 and even 95% with no signs of membrane scaling (Fig. 5 c and d). The advantages of WAC-IEX pre-treatment identified in the preliminary experiments (chapter 3.1.2) were further confirmed upon coupling IEX with subsequent RO operation, yielding significantly lower calcite supersaturation at 90% recovery (e.g., SI < 1 for WAC-IEX versus SI > 2 for SAC-IEX), see Fig. 5 a) and c). The linear permeability decline in the WAC-IEX case is presumably caused by organic fouling, since the concentrate DOC reaches about 30 mgC/L and 60 mgC/L at 90% and 95% recovery, respectively. Mitigation strategies are discussed later in this chapter, exemplified by CCRO operation.

To further assess the influence of SAC and WAC pre-treatment, the observed rejection (Fig. 5 e) was evaluated based on the overall same conditions (pre-treatment 50:50, 90% recovery, 20 LMH). Therefore, the rejection of salts (based on EC measurement), TIC, and characteristic ions were determined. The hardness was excluded from the analysis because the permeate concentrations of calcium and magnesium were below the LOQ. The WAC configuration exhibited an overall higher salt rejection, resulting in a 20% lower permeate TDS. This is surprising considering the positive effect of elevated pH on the rejection (see Fig. 3 d) and the significantly higher concentrate pH of the SAC (7.92) compared to WAC (7.10) configuration. The enhanced performance is presumably linked to the change of the ion composition. For once, SAC

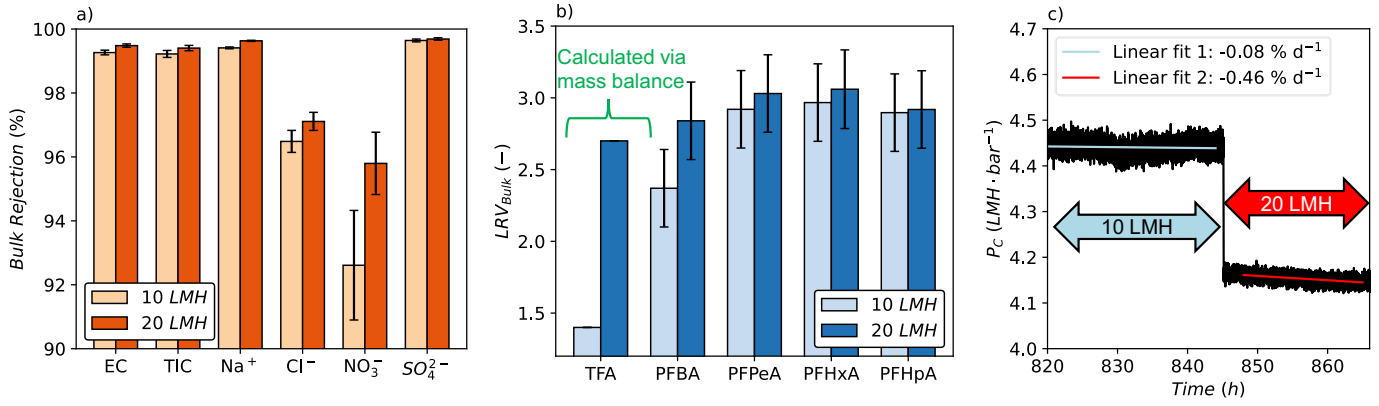


Fig. 4. Exp. 1.2.: Influence of flux on rejection of a) EC, TIC and selected ions, b) selected PFAS (TFA is calculated based on a mass balance, see eq. (4)) and c) permeability curve.

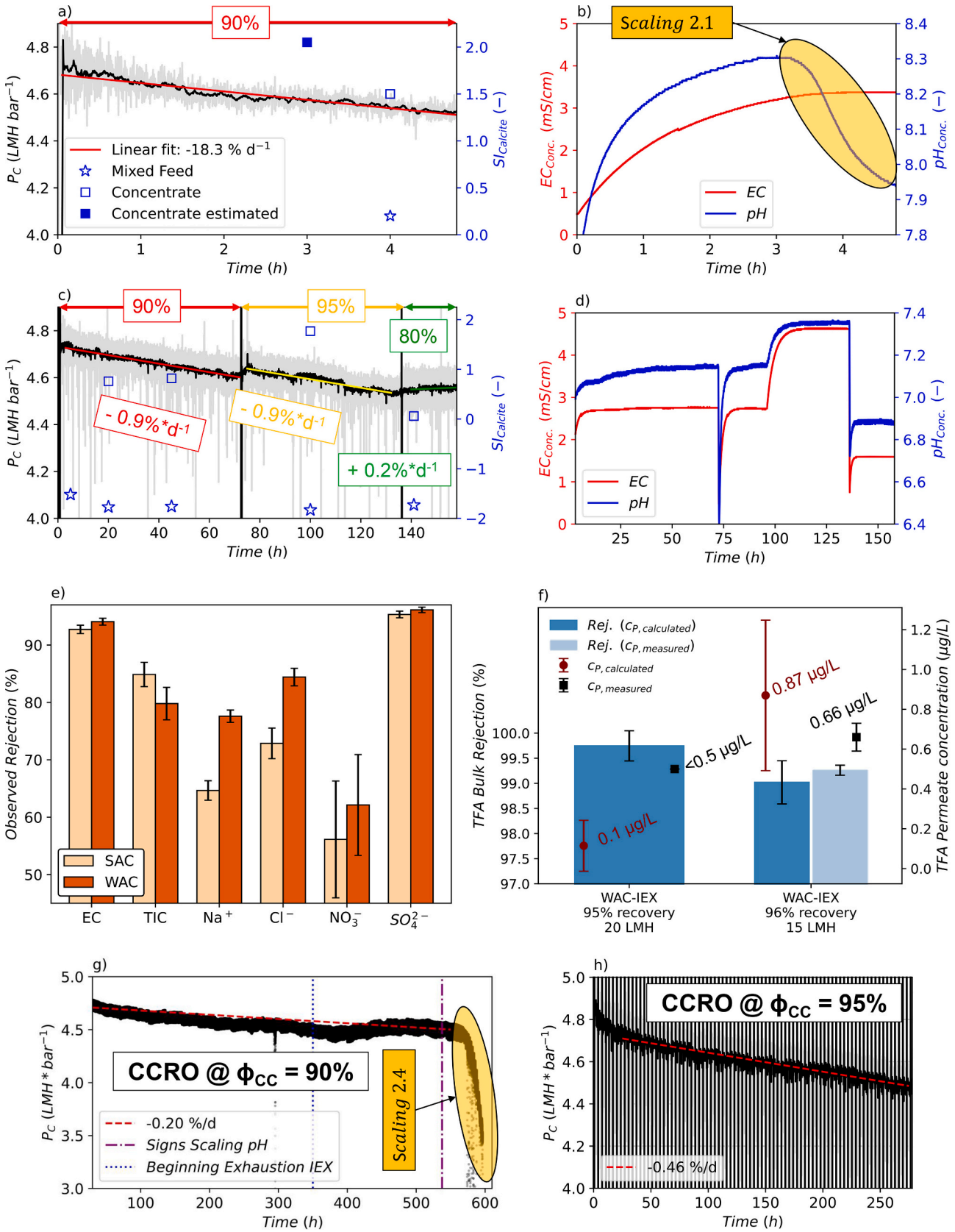


Fig. 5. Corrected permeability Pc with raw data (grey) and rolling mean (black), calcite SI, concentrate EC and pH over time for: SAC- (a, b) and WAC-IEX (c, d) pre-treatment, each with 50% bypassed and 50% softened feed; SAC-IEX at 90% recovery, WAC-IEX at 90, 95 and 80% recovery; e)Comparison of SAC and WAC pre-treatment at 90% recovery for observed rejection of EC, TIC, selected ions; f) TFA rejection; g) and h) CCRO operation with 50% WAC-IEX pre-treatment at 90 and 95% closed-circuit recovery (ϕ_{CC});

softening produces a higher ionic strength effluent compared to WAC, see Table 3. An increase in ionic strength enhances charge screening, which may partially offset the beneficial effect of elevated pH in the SAC configuration, thereby leading to reduced rejection. Secondly, the application of SAC-IEX leads to an increase in monovalent sodium concentration, resulting in an approximately fourfold higher sodium concentration in the SAC-IEX configuration. As monovalent ions are generally less retained, this may contribute to the reduced permeate quality in case of the SAC-IEX configuration. The lower TIC removal in the WAC configuration is attributed to a higher fraction of uncharged CO_2 in the feed.

In general, the results indicate that WAC-IEX offers significant advantages over SAC-IEX pre-treatment, which are discussed in detail in chapter 3.2.3.

The PFAS rejection of the WAC configuration was evaluated at a recovery of 95%. No PFAS were detected in the permeate samples, as all concentrations remained below the respective LOQ (< 1 ng/L for PFAS-20). Consequently, the minimum rejection was estimated using the LOQ values (see Supplementary Information Fig. S6). Moreover, TFA bulk rejection of the WAC configuration was evaluated at a recovery of 95% at 20 LMH and at 96% recovery at 15 LMH, see Fig. 5 f). At 95% recovery, TFA permeate concentrations were below the LOQ, so a mass balance was applied (see eq. (4)), indicating bulk rejections approaching three log units (≈99.9%). At 96% recovery, TFA was detectable in the permeate. Due to the lower flux, the bulk rejection is substantially reduced, highlighting the strong influence of flux on the removal of ultra-short-chain PFAS, see also Fig. 4 b.

It should be noted that the system was operated under a worst-case scenario in feed-and-bleed mode. Under these conditions, the RO element is continuously exposed to elevated concentrations, in contrast to typical full-scale practice where multi-stage configurations are employed and a concentration profile develops along the plant length. This operating mode largely explains the comparatively low rejection observed for certain ions, such as nitrate. Nevertheless, it is noteworthy that, despite these harsh conditions, PFAS-20 were detected in the permeate only for raw water 1, and even in this case, typical regulatory limit values were still met (at 20 LMH see supplement Fig. S5), highlighting the strong PFAS removal performance of standard commercial RO membranes.

Finally, in Exp. 2.3 and 2.4, the plant was operated with WAC pre-treatment (50:50) and CCRO operation. The objective was to determine whether it would be possible to mitigate the permeability drop in conventional operation that occurs due to organic fouling. Fig. 5 g) displays CCRO operation at 90% closed-circuit recovery (ϕ_{CC}), which had approximately 80% less permeability drop compared to continuous operation, see Fig. 5 c), over 500 h operation. The same findings emerged in another study we conducted. Here we hypothesized that this is related to a less compact fouling layer, due to process inherent frequent flushing in CCRO operation, which allows to (partially) shear off formed fouling layers in flushing intervals [30].

Furthermore, the plant was operated beyond the exhaustion of the IEX to ascertain a robust and stable operation even under these harsh conditions. It was confirmed that the system continued to operate for approximately 200 additional hours without any indications of scaling. As in our previous studies [30,31], the first signs of $CaCO_3$ scaling were observed in the concentrate pH. Approximately 30 h later, a substantial decline in permeability was detected. The relatively long period (≈ 200 h) of stable operation following exhaustion is due to the fact that the IEX continuing to soften the water to a certain extent (about another 50 h) as well as to frequent inherent flushing, which (partially) removes deposits [30,46].

Moreover, CCRO operation at 95% recovery exhibited a 50% lower permeability decline compared to continuous operation, see Fig. 5 h). Another advantage of CCRO operation in this case was that flushing was not carried out with the mixed feed (50% raw water and 50% softened water), but exclusively with raw water, thereby further reducing the consumption of softened water. However, it must be noted that, due to the experimental scale (characterized by a high ratio of system volume to membrane surface area and relatively slow valve actuation leading to long transition phases), CCRO performance was evaluated using the closed-circuit recovery. This approach excludes the influence of flushing (see chapter 2.4) on recovery due to the loss of water and production time. However, with respect to productivity, defined as the ratio of filtration time (closed-circuit mode) to flushing time, both typical (25:1 to 100:1) and very high productivity (up to 215:1) settings were applied, with the latter clearly exceeding values commonly reported in the literature, e.g., 80:1 and 90:1 [47]. Therefore, the plant availability (filtration time to total time) was high, ranging from 96 to 99.5%, allowing transfer to full-scale applications. Further experiments were carried out to increase the attainable recovery, enabling operations up to even 98.4% closed-circuit recovery (see Supplementary Information Fig. S7).

3.2.3. Comparative assessment and implications for IEX selection

For the raw waters studied, which have a high fraction of carbonate hardness, both the batch experiments and the hybrid IEX-RO treatment system demonstrated advantages of WAC-IEX in reducing calcite saturation.

By reducing calcite saturation, WAC-IEX allows for higher RO recovery rates or a reduced pre-treatment stream, enabling cost-effective partial softening in bypass mode. Combined with the higher operating capacity and lower regenerant consumption reported in the literature [25,48], this leads to a significant reduction in brine production compared to SAC-IEX, which represents a major bottleneck in IEX applications [25]. As shown by the exemplary calculation in Chapter 2.2 of the Supplementary Information, partial softening using WAC-IEX would reduce both the required resin volume and brine production by 75% compared with full-stream SAC softening, while achieving the same calcite saturation. Moreover, WAC resins can be regenerated with CO_2, either alone or in combination with anion exchange, enabling simultaneous cation and anion removal (CARIX process; [49]), which improves concentrate management by reducing both salinity loading and the use of hazardous chemicals compared with conventional acid regeneration (e.g., HCl for WAC).

In the case of SAC-IEX, the use of non-hazardous NaCl as regenerant and the combination with downstream RO offer the additional possibility of utilizing the RO concentrate for partial regeneration, thereby reducing the overall demand for chemicals [21–23]. Although regeneration effectiveness strongly depends on feed-water composition, efficient regeneration generally requires a high proportion of monovalent relative to multivalent cations [21,22].

In addition, the effects on subsequent RO operation vary. The WAC-IEX pretreatment slightly improved the rejection of conventional water constituents (Fig. 5 e), while PFAS retention, which was evaluated under various pH conditions, remained largely unaffected (Fig. 3 f). For SAC-IEX, however, the near-complete removal of total hardness can offer additional operational benefits, particularly when combined with a downstream RO process, e.g., to lower the risk of organic fouling [38]. This is particularly relevant for waters with high potential for organic fouling, as discussed in chapter 3.2.1.

Another advantage of the hybrid WAC-IEX/RO setup is the substantially lower TDS content in the IEX effluent and the resulting reduction in osmotic pressure, see Table 3. This yields in a significantly lower specific energy consumption. As shown in Chapter 2.2 of the Supplementary Information for various scenarios, partial WAC softening could reduce the specific energy consumption (SEC) by approximately 8%, while the savings would increase to up to 15% with complete WAC softening.

3.2.4. Concentrate treatment for PFAS removal

Fig. 6 a) to h) compares PerfluorAd® treatment of raw water 1 (open markers) and its RO concentrate (filled markers), both with an

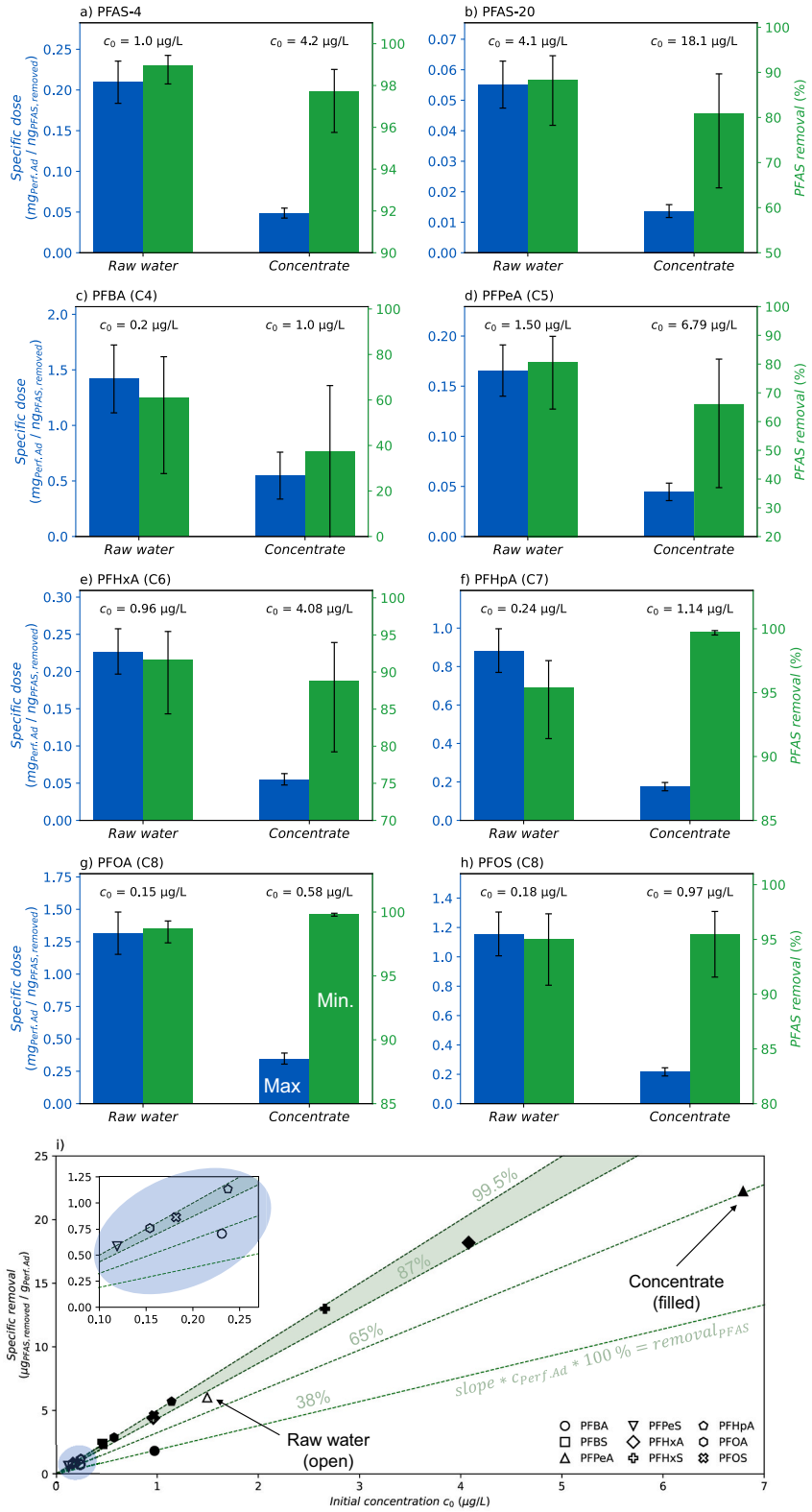


Fig. 6. PerfluorAd® (0.2 g/L) and $FeCl_3$ (0.01 g/L) application for raw water and concentrate treatment. Comparison of specific PerfluorAd® dose (blue bars) and PFAS removal (green bars); For PFOA (g) the concentrate specific dose and removal is based on the LOQ; i) Initial dose as a function of initial PFAS concentration and j) specific removal as a function of initial PFAS concentration for various PFAS in raw water (hollow markers) and concentrate (filled markers); Data shown are based on experiments with raw water 1 and the respective generated concentrates; Black error-bars for PFAS-removal display the maximum error. (For interpretation of the references to colour in this figure legend, the reader is referred to the web version of this article.)

equivalent dosing concentration of 0.2 g/L, illustrating specific dose (blue bars) and removal (green bars) of PFAS sum parameters (a, b) as well as selected individual PFAS (c - h). The specific dose of PerfluorAd® is lower in each case when treating the concentrate, reflecting the greater absolute reduction in PFAS contamination compared to raw water; for example, this reduction is approximately fivefold for PFHpA and PFOS.

However, the achieved removal efficiencies vary. This is especially evident for the shorter carboxylic PFAS (PFBA and PFPeA), where removal from the concentrate is lower, which in turn is reflected in the overall PFAS-20 removal efficiency. On the other hand, for longer chain PFAS, the removal is comparable (PFAS-4, PFHxA, PFOS) or even elevated for the concentrate (PFHpA, PFOA). Interestingly, in the case of PFHpA and PFOA the removal is not only relatively higher but also absolutley. For instance, the concentration of PFHpA in the concentrate after treatment with PerfluorAd® is more than three times lower than after treatment of the raw water.

Overall, a strong linear relationship between the initial concentration and the specific dose was observed. Fig. 6 i) displays the specific removal of individual PFAS versus their initial concentration, together with linear fits through the origin with different slopes. The slope is directly proportional to the PFAS removal and can be obtained by multiplying the slope by the PerfluorAd® dose (0.2 g/L). Most of the PFAS data points lie between the lines corresponding to 87% and 99.5% removal (filled area). This linear trend indicates that increasing the recovery, and thus the hydraulic concentration factor, will reduce the required PerfluorAd® mass to achieve comparable PFAS removal, demonstrating that the initial concentration strongly governs the specific dose and confirming reports of higher efficiency of concentrate treatment compared to raw water treatment [7].

Data points outside the filled area between 87 and 99.5% removal correspond to PFBA and PFPeA, observed in both the raw water and the concentrate. This can be explained, first, by the short chain length of these PFAS (C_4 and C_5). Shorter perfluorinated carbon chains are more hydrophilic (lower octanol water coefficient log K_{OW}) and more mobile (higher diffusivity) [13,50], which increases polarity and water solubility and, in turn, reduces their sorption and aggregation tendency into the PerfluorAd® flocs. Moreover, the functional group is decisive, as illustrated by the fact that the removal of short-chain PFBS, in contrast to PFBA, is still in the area between 87 and 99.5%. Sulfonate functional groups induce a higher neagtive charge potentially boosting sorption [50]. The phenomenon of higher removal of sulfonic acids compared to carboxylic acids at the same chain length is well documented in the literature across various treatment methods, e.g., leading to faster break through of carboxylic PFAS in fixed bed treatment, e.g., ion exchange or activated carbon [50–52].

With regard to the practical implications of the results, it can be concluded that, at identical, or comparable removal efficiencies and PerfluorAd® concentrations in raw-water and concentrate treatment (e.g., for PFHxA and PFOS), the same PFAS mass load is removed. However, in the case of concentrate treatment, the same PFAS load can be removed with a lower PerfluorAd® mass, in proportion to the hydraulic concentration factor. As an example, at a recovery of 75%, the dosed PerfluorAd® mass is reduced fourfold, whereas at 90% recovery it is reduced by a factor of 10. With even higher removal efficiencies, as observed for longer-chain PFAS (PFHpA, PFOA), the potential to reduce the required PerfluorAd® dose in concentrate treatment becomes particularly evident. A simple example comparing raw water and concentrate treatment is provided in the Supplementary Information (Fig. S8) for three selected PFAS, showing equal (PFOS), higher (PFHpA), and lower (PFBA) removal in concentrate treatment compared with raw water treatment. This example therefore illustrates both the advantages and potential drawbacks of concentrate treatment. The advantages are particularly apparent in the substantially lower PerfluorAd® demand and, for some PFAS, the potentially higher absolute PFAS mass removal and even lower effluent concentrations. However, for PFAS exhibiting comparable removal in raw water and concentrate treatment, the absolute PFAS mass removed is similar, whereas the residual concentration following concentrate treatment remains higher because of the elevated influent concentration. This raises an important regulatory question as to whether treatment performance should primarily be evaluated in terms of PFAS mass-load reduction or compliance with concentration-based discharge limits. Furthermore, where removal is lower during concentrate treatment, the residual PFAS concentration may exceed the initial concentration in the raw water, depending on the RO recovery. This may be of particular concern for PFAS such as PFBA if the treated concentrate is discharged, see the example in supplement Fig. S8.However, it should be noted that PerfluorAd® is generally not designed to target short-chain PFAS. For medium- (PFHpA) and long-chain (PFOS) PFAS, comparable or even superior removal efficiencies were achieved when treating the concentrate rather than the raw water, highlighting the potential of concentrate treatment. Furthermore, discharge regulations for generated drinking water concentrates, such as the wastewater ordinance and generally accepted rules of technology, currently do not define PFAS limits. To the best of the authors knowledge, the only existing regulation for such a facility goes beyond standard requirements by enforcing a discharge limit based on long chain PFOA (< 100 ng/L [6]). Thus, comparing concentrate and raw water treatment with regard to a PFOA threshold reveals clear advantages for concentrate treatment using PerfluorAd®, as higher relative and absolute removal performance is achieved with a lower specific dosage, see Fig. 6 g.

Additional experiments using a range of PerfluorAd® dosages are required to further clarify how recovery affects treatment performance when target threshold values must be met. These experiments should also evaluate the potential consequences of overdosing in the raw water and underdosing in the concentrate, as well as the potential advantages of two-stage treatment configurations.

Adsorption tests using PAC were conducted with raw water 1 and the concentrates generated from it, as well as with concentrates derived from raw water 2 produced at different recovery rates, to investigate the impact of the recovery. Fig. 7 a), c) – h) depict the adsorption capacity (q) as function of the equilibrium concentration (c_{eq}) for PFAS-20 and selected individual PFAS. It can be seen that the adsorption capacity generally increases with recovery. Moreover, the PFAS adsorption capacity of waters originating from raw water 1 is significantly higher.

PFBA exhibits the lowest adsorption capacity (Fig. 7 c) in both waters due to its short chain length, high polarity, and weak hydrophobic and electrostatic interactions with PAC, in contrast to PFBS (Fig. 7 d), which adsorbs more strongly owing to its sulfonate group. Notably, PFBA shows no initial adsorption for raw water 2 but exhibits measurable uptake at higher recoveries, indicating a concentration-driven effect. The absence of uptake at low initial concentrations is likely due to pronounced matrix and competition effects combined with the inherently low sorption affinity of short-chain PFAS, such that a minimum PFBA concentration must be exceeded before electrostatic and non-electrostatic interactions become sufficiently effective to yield a measurable net uptake despite the simultaneous enrichment of competing substances. The positive effect of increasing recovery on PAC treatment of the concentrate, specifically regarding short chain PFBA, is shown in Fig. S9 of the Supplementary Information, highlighting the potential to improve short chain PFAS removal at elevated recoveries.

The highest adsorption capacity for raw water 1 is found for the C_6-PFAS, namely PFHxA and PFHxS, with 25 and 40 ng/mg, respectively, exceeding raw water 2 by factor 200 and 100, respectively. The high adsorption capacities for PFHxA and PFHxS in raw water 1 are likely a concentration effect, indicated by the high equilibrium concentrations. In contrast, the long-chain PFAS, PFOA and PFOS, show the highest adsorption in raw water 2, which correlates with relatively high equilibrium concentration, too.

Given that the initial PFAS concentration of raw water 1 is considerably higher than that of raw water 2 (see Fig. 7 i and j), the typically

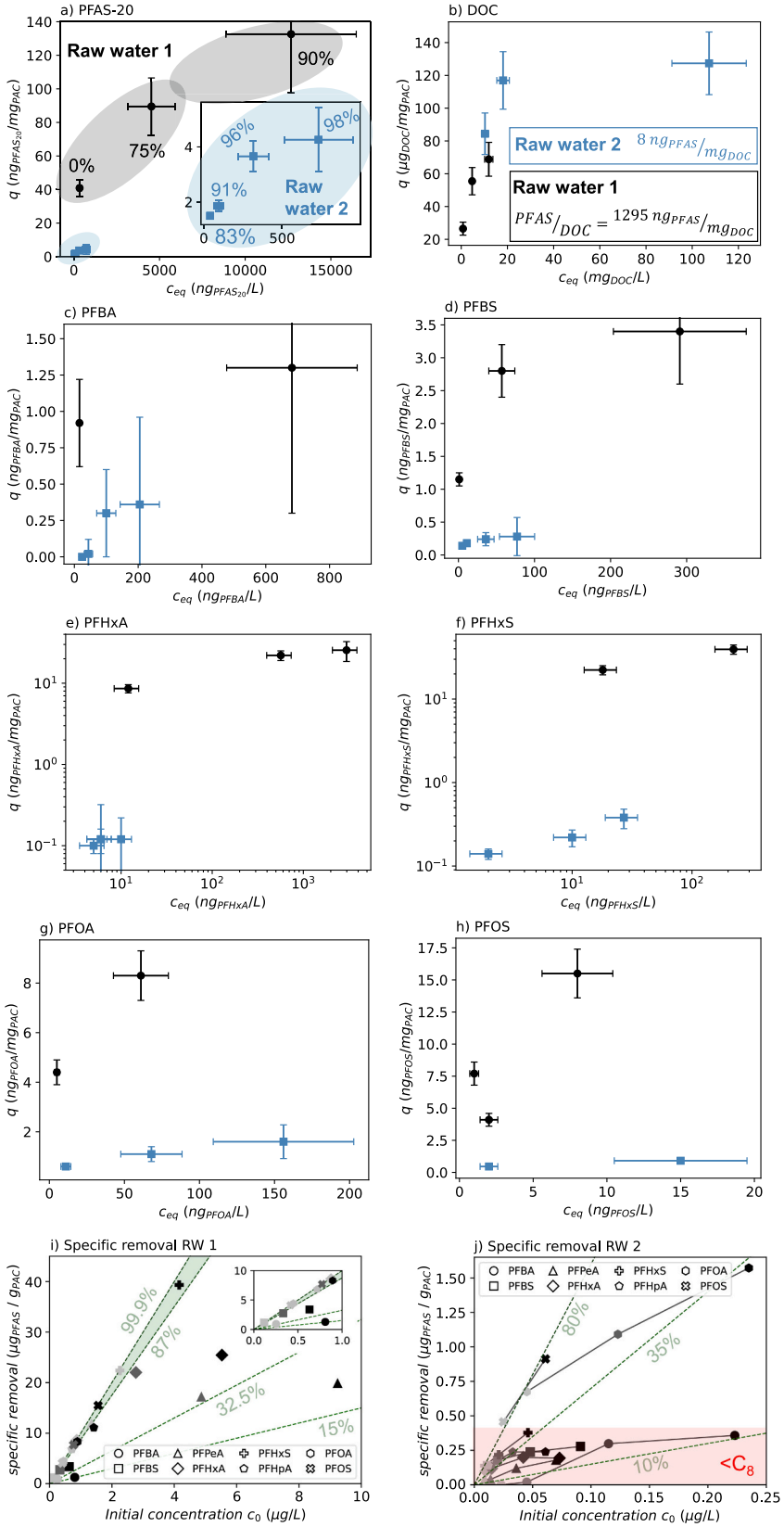


Fig. 7. PAC adsoprtion tests applying 100 mg/L (raw water 1 and generated concentrates) and 50 mg/L (concentrates generated from raw water 2): a) to h) loading vs. equilibrium concentration for raw water 1 (black) and 2 (blue); i) and j) specific removal vs. initial concentration

higher equilibrium concentration provides a greater driving force for adsorption and may thus explain the significantly higher adsorption capacity observed for raw water 1. However, since the concentrates of raw water 2 were produced at significantly higher recoveries, the equilibrium concentration in some cases matches or even exceeds that of raw water 1. For instance, raw water 1 has an equilibrium concentration of PFAS-20 that is comparable to the concentration of the concentrate generated at 96% recovery of raw water 2 (300 ng/L). However, raw water 1 has a 10-fold higher adsorption capacity. A comparison of the concentrates of PFOS in raw water 1 and 2 reveals that raw water 2 has an 8-fold higher equilibrium concentration, yet an approximately 17-fold lower adsorption capacity. Therefore, differences in initial concentration are unlikely to account for the observed performance, and an influence of the different water matrices appears more plausible.

A comparison of the concentrates at the highest recovery application for raw water 1 and 2 indicates that the concentrate from raw water 2 yields approximately double the ionic strength. Abulikemu et al. [53] showed that ionic strength has a significant impact on GAC performance, with reduced ionic strength markedly improving PFAS removal. The effect of ionic strength is primarily explained by the weakening of electrostatic interactions between the sorbent and PFAS due to compaction of the electrical double layer and is elevated for short chain PFAS [53,54]. Moreover, the organic background may also contribute. The adverse effect of natural organic matter on micropollutant adsorption, arising from competitive adsorption [55], has been extensively reported, as organic matter occupies adsorption sites and thus reduces the effective adsorption capacity of the sorbent for target compounds [56], in particular for short-chain PFAS [14]. Haist-Gulde [57] reported significantly faster breakthrough of PFAS-4 in GAC filtration at elevated concentrations of DOC in the feed water. However, the DOC concentration of raw water 1 is higher than that of raw water 2 (approximately 20%). Still raw water 1 outperforms raw water 2.

Considering the adsorption isotherms of the DOC for both waters, see Fig. 7 b), reveals higher DOC adsorption capacity of raw water 2 compared to raw water 1. Therefore, significant variations in performance can likely be attributed to the organic background, particularly given the fact that the fraction of PFAS to DOC is over 160 times higher in raw water 1 than in raw water 2. This suggests less competition with DOC in raw water 1 compared to raw water 2. The evaluation of the fraction of the sum of PFAS to the DOC might be an effective parameter to estimate the adsorption performance, though more research is needed, in particular advanced characterization of the DOC, e.g., by LC-OCD.

Finally, in analogy to the PerfluorAd® application, the specific PFAS removal was plotted versus the initial concentration for raw waters 1 and 2, see Fig. 7 i) and j). Increasing marker darkness denotes higher initial concentrations (higher recovery), and the slopes of the straight lines through the origin quantify the respective removal.

For raw water 1, most PFAS follow a linear trend, with slopes corresponding to 87–99.9% removal, demonstrating the same positive effect of higher concentration as noticed for PerfluorAd®. However, in contrast to PerfluorAd®, the PAC application appears to be more PFAS-compound-specific: For PFHxA, PFPeA and PFBS, a saturation-like increase is observed, i.e., a pronounced deviation from the linear trend, indicating that with increasing concentration (and thus recovery) the gain in specific removal progressively diminishes. This behavior is also evident for PFBA: increasing the initial concentration only slightly enhances the specific removal, while the overall removal efficiency decreases markedly, for example from 40 to 15% upon a threefold increase in concentration.

For raw water 2, a clear separation between long-chain and short-chain PFAS becomes evident: the specific removal of long-chain compounds such as PFOA and PFOS is substantially higher, whereas PFAS with fewer than eight carbon atoms show much lower specific removal, even at elevated initial concentrations. In general, the overall removal achieved for raw water 2 is markedly lower than for raw water 1, and no clear linear trend in specific removal with increasing initial concentration is observable. This behavior indicates pronounced matrix effects, most likely driven by competition with DOC for adsorption sites, see Fig. 7 b).

It should be noted that although increasing recovery enhanced concentrate treatment via PAC, yielding higher PFAS adsorption capacity, the overall removal efficiency decreased (see, e.g., Fig. S9 a in the Supplementary Information for PFAS-20). However, for fixed-bed GAC systems, this lower batch removal has no practical impact. Due to the development of a moving mass-transfer zone along the filter bed, near-complete removal efficiency is maintained, albeit with a faster breakthrough of short-chain compounds due to significant lower loading [6]. Given that GAC is already applied for concentrate treatment [6], the higher loading achieved at elevated recoveries might substantially extend bed service life or reduces specific carbon consumption. Interestingly, a pronounced increase in recovery (e.g., from 75 to 90% for raw water 1 and from 90 to 96% for raw water 2) led to a substantial increase in PFAS-20 loading, almost mirroring the rise in the concentration factor, see Fig. 7 a) and Fig. S9 a) in the supplement. Thereby, this study highlights the potential of high-recovery operations to enhance the economics of increasingly relevant concentrate treatment for micropollutant removal prior to discharge.

4. Conclusion

This study investigated strategies to improve membrane-based treatment of PFAS-contaminated waters by addressing both PFAS retention and concentrate management for two real water matrices prone to $CaCO_3$ scaling and organic fouling, with contrasting PFAS contamination levels on a technical scale. It was hypothesized that high recovery operation is advantageous for downstream treatment; therefore, SAC and WAC ion exchange (IEX) were evaluated as pre-treatment options to enable high recoveries without the use of antiscalants. The following conclusions can be drawn:

- WAC-IEX offers advantages over SAC-IEX as a pre-treatment step for water that causes $CaCO_3$ scaling, especially because of
  - o higher reduction of SI, which allows higher recoveries or less pre-treatment,
  - o lower effluent TDS, yielding in lower osmotic pressure for RO operation and lower RO permeate TDS.
- CCRO operation showed less organic fouling compared to continuous operation.
- The investigated typical brackish water RO membrane (BW30) achieved bulk rejections near 3 log units for common long- and short-chain PFAS and, even for TFA, approaching 2.5 log units at a design flux of 20 LMH under “worst-case” feed-and-bleed operation
- Both concentrate treatment (vs. raw water treatment) and higher recovery operation increased specific removal for PerfluorAd® and PAC, indicating more effective load removal during concentrate treatment with reduced chemical demand. This effect was most pronounced for long-chain PFAS, where concentrate treatment partly achieved higher absolute removal than raw water treatment.
- However, particularly for short-chain PFAS, higher load removal at increased recovery was accompanied by lower removal efficiencies. Therefore, if it is necessary to assess compliance with limit values, further studies are required to evaluate the effects of recovery, for example by testing different sorbent dosages or evaluating two-stage treatment concepts.
- While higher recoveries may reduce removal efficiency in single-stage PAC and PerfluorAd® systems, the resulting elevated loadings may enhance practically relevant GAC bed service life and lower carbon demand, demonstrating the potential of high-recovery operations to improve the economics of concentrate treatment.

- The water matrix is decisive for concentrate post-treatment, in particular the ratio of DOC to PFAS, presumably due to competitive DOC adsorption.
- PFAS may adsorb on $CaCO_3$ precipitates, which should be further investigated.

CRediT authorship contribution statement

Martin Futterlieb: Writing – review & editing, Writing – original draft, Visualization, Validation, Supervision, Software, Methodology, Investigation, Funding acquisition, Formal analysis, Data curation, Conceptualization. **Mirjana Futterlieb:** Writing – review & editing, Resources, Project administration, Methodology, Investigation, Data curation. **Peter Leube:** Investigation, Data curation. **Avner Ronen:** Writing – review & editing, Funding acquisition. **Stefan Panglisch:** Writing – review & editing, Validation, Supervision, Resources, Project administration, Funding acquisition.

Declaration of generative AI and AI-assisted technologies in the writing process

The author's original draft was edited with DeepL, Gemini and Perplexity Pro to improve grammar, expression, and readability. Moreover, Perplexity Pro was used for troubleshooting in data processing using Python. The literature survey was supported by Google Scholar Labs. After using these tools, the authors reviewed and edited the content as needed and took full responsibility for the publication's content.

Declaration of competing interest

The authors declare that they have no known competing financial interests or personal relationships that could have appeared to influence the work reported in this paper.

Acknowledgments

The authors gratefully acknowledge financial support from the BMBF–MOST cooperation project DEFEAT PFAS (grant no. 02WIL1660A). The reverse osmosis (RO) and ultrafiltration (UF) systems were partially funded by the European Regional Development Fund (EFRE) under the EFRE-NRW 2014–2020 program. The authors sincerely thank Endress+Hauser GmbH+Co. KG, particularly Lars Bondzio and Dr. Achim Gahr, for their cooperation and for providing measurement equipment essential to this study. The authors gratefully acknowledge Dr. Jochen Henkel (DuPont) for supplying the reverse osmosis membranes used in this study. We also acknowledge Cornelsen Umwelttechnologie GmbH for their support and for supplying PerfluorAd® as well as contaminated water samples. Special thanks are extended to Dr. Martin Cornelsen, Dr. Verena Stenert, and Karsten B. Schwarz for their valuable collaboration. We also gratefully acknowledge the support of Lanxess AG, particularly Björn Dinges, for supplying the ion exchange resins. We thank Puneet Naresh Manghnani and Antonia Charalampidi for their experimental contributions. Finally, we would like to thank the anonymous reviewers for their insightful feedback, which significantly helped improve the quality of the manuscript.

Appendix A. Supplementary data

Supplementary data to this article can be found online at https://doi.org/10.1016/j.seppur.2026.140303.

Data availability

Data will be made available on request.

References

[1] T.D. Appleman, C.P. Higgins, O. Quiñones, B.J. Vanderford, C. Kolstad, J. C. Zeigler-Holady, E.R.V. Dickenson, Treatment of poly- and perfluoroalkyl substances in U.S. full-scale water treatment systems, Water Res. 51 (2014) 246–255, https://doi.org/10.1016/j.watres.2013.10.067.
[2] Q. Ma, Q. Lei, F. Liu, Z. Song, B. Khusid, W. Zhang, Evaluation of commercial nanofiltration and reverse osmosis membrane filtration to remove per-and polyfluoroalkyl substances (PFAS): effects of transmembrane pressures and water matrices, Water Environ. Res. 96 (2024) e10983, https://doi.org/10.1002/wer.10983.
[3] C.J. Liu, G. McKay, D. Jiang, R. Tenorio, J.T. Cath, C. Amador, C.C. Murray, J. B. Brown, H.B. Wright, C. Schaefer, C.P. Higgins, C. Bellona, T.J. Strathmann, Pilot-scale field demonstration of a hybrid nanofiltration and UV-sulfite treatment train for groundwater contaminated by per- and polyfluoroalkyl substances (PFASs), Water Res. 205 (2021) 117677, https://doi.org/10.1016/j.watres.2021.117677.
[4] J. Thompson, G. Eaglesham, J. Reungoat, Y. Poussade, M. Bartkow, M. Lawrence, J.F. Mueller, Removal of PFOS, PFOA and other perfluoroalkyl acids at water reclamation plants in south East Queensland Australia, Chemosphere 82 (2011) 9–17, https://doi.org/10.1016/j.chemosphere.2010.10.040.
[5] M. Scheurer, K. Nödler, F. Freeling, J. Janda, O. Happel, M. Riegel, U. Müller, F. R. Storck, M. Fleig, F.T. Lange, A. Brunsch, H.-J. Brauch, Small, mobile, persistent: Trifluoroacetate in the water cycle – overlooked sources, pathways, and consequences for drinking water supply, Water Res. 126 (2017) 460–471, https://doi.org/10.1016/j.watres.2017.09.045.
[6] S. Stauder, U. Müller, S. Egner, P. Riedinger, PFAS-Entfernung mit Umkehrosmose und Aktivkohle, Energie Wasser-Prax. 09 (2024).
[7] V. Franke, P. McCleaf, K. Lindegren, L. Ahrens, Efficient removal of per- and polyfluoroalkyl substances (PFASs) in drinking water treatment: nanofiltration combined with active carbon or anion exchange, Environ. Sci. Water Res. Technol. 5 (2019) 1836–1843, https://doi.org/10.1039/c9ew00286c.
[8] V. Franke, M. Ullberg, P. McCleaf, M. Wålinder, S.J. Köhler, L. Ahrens, The Price of really clean water: combining Nanofiltration with granular activated carbon and anion exchange resins for the removal of per- and Polyfluoroalkyl substances (PFASs) in drinking water production, ACS ES&T Water 1 (2021) 782–795, https://doi.org/10.1021/acsestwater.0c00141.
[9] E.W. Tow, M.S. Ersan, S. Kum, T. Lee, T.F. Speth, C. Owen, C. Bellona, M. N. Nadagouda, A.M. Mikelonis, P. Westerhoff, C. Mysore, V.S. Frenkel, V. deSilva, W.S. Walker, A.K. Safulko, D.A. Ladner, Managing and treating per- and polyfluoroalkyl substances (PFAS) in membrane concentrates, AWWA Water Sci. 3 (2021) e1233, https://doi.org/10.1002/aws2.1233.
[10] A. Röhrig, N. Grasse, M. Krauss, D. Bücher, W. Brack, N. Kamjunke, A. Matousu, T. Sanders, I. Bussmann, E.P. Achterberg, T. Reemtsma, Q. Fu, Beyond legacy PFAS: dominant role of ultrashort-chain and emerging PFAS in the Elbe River–sea continuum, ACS Environ. Au 6 (2026) 421–434, https://doi.org/10.1021/acsenvironau.5c00219.
[11] A. Safulko, T.Y. Cath, F. Li, B. Tajdini, M. Boyd, R.P. Huehmer, C. Bellona, Rejection of perfluoroalkyl acids by nanofiltration and reverse osmosis in a high-recovery closed-circuit membrane filtration system, Sep. Purif. Technol. 326 (2023), https://doi.org/10.1016/j.seppur.2023.124867.
[12] N.A. Masters, B.A. Marron, A. Lau, W.G. Bailey, S.D. Richardson, C.L. Bellona, Investigation of PFAS rejection by closed-circuit reverse osmosis and nanofiltration and sorption to treatment materials during groundwater treatment: a pilot demonstration, Sep. Purif. Technol. 377 (2025) 134308, https://doi.org/10.1016/j.seppur.2025.134308.
[13] J. Cao, S. Feng, A.A. Dolatabad, Y. Zhi, B. Deng, C. Liu, X. Lyu, C.S.Q. Christensen, J.J. Pignatello, P. Ni, S. Lin, Z. Wei, F. Xiao, PFAS removal from reverse osmosis and nanofiltration brine by granular activated carbon: thermodynamic insights into salinity effects, Water Res. 282 (2025) 123758, https://doi.org/10.1016/j.watres.2025.123758.
[14] A. Meservey, M. Mitchek, J. Wong, K.D. Pennell, Competitive adsorption of per- and polyfluoroalkyl substances (PFAS) on activated carbon: impact of activated carbon and PFAS properties, J. Hazard. Mater. 505 (2026) 141462, https://doi.org/10.1016/j.jhazmat.2026.141462.
[15] S.A. Kaushik, D. Armbruster, J. Dittmer, D. Bruniecka-Sulewski, B. Wendler, M. Ernst, Investigation of scaling inhibition and biofouling potential of different molecular weight fractions of a PAA antiscalant, Npj Clean Water 7 (2024) 36, https://doi.org/10.1038/s41545-024-00332-7.
[16] R. Kuhn, C. Vornholt, V. Preuss, I.M. Bryant, M. Martienssen, Aminophosphonates in Nanofiltration and reverse osmosis permeates, Membranes-Basel 11 (2021), https://doi.org/10.3390/membranes11060446.
[17] BMBF, Abschlussbericht KonTriSol: Konzentrate aus der Trinkwasseraufbereitung – Lösungsansätze für die technischen, rechtlichen und wirtschaftlichen Hemmnisse beim Einsatz von NF/UO-Prozessen in der Trinkwasseraufbereitung, 2023.
[18] D. Armbruster, U. Müller, O. Happel, Characterization of phosphonate-based antiscalants used in drinking water treatment plants by anion-exchange chromatography coupled to electrospray ionization time-of-flight mass spectrometry and inductively coupled plasma mass spectrometry, J. Chromatogr. A 1601 (2019) 189–204, https://doi.org/10.1016/j.chroma.2019.05.014.
[19] L.F. Greenlee, F. Testa, D.F. Lawler, B.D. Freeman, P. Moulin, The effect of antiscalant addition on calcium carbonate precipitation for a simplified synthetic brackish water reverse osmosis concentrate, Water Res. 44 (2010) 2957–2969, https://doi.org/10.1016/j.watres.2010.02.024.
[20] DuPont, FilmTec™ Reverse Osmosis Membranes Technical Manual, 2024.
[21] M. Vanoppen, G. Stoffels, J. Buffel, B. De Gusseme, A.R.D. Verliefde, A hybrid IEX-RO process with brine recycling for increased RO recovery without chemical

addition: a pilot-scale study, Desalination 394 (2016) 185–194, https://doi.org/10.1016/j.desal.2016.05.003.
[22] M. Vanoppen, G. Stoffels, C. Demuytere, W. Bleyaert, A.R.D. Verliefde, Increasing RO efficiency by chemical-free ion-exchange and Donnan dialysis: principles and practical implications, Water Res. 80 (2015) 59–70, https://doi.org/10.1016/j.watres.2015.04.030.
[23] M. Futterlieb, I.M.A. ElSherbiny, M. Tuczinski, J. Lipnizki, S. Panglisch, Limits of high recovery inland desalination: closed-circuit reverse osmosis – a viable option? / 93 (2021) 1359–1368, https://doi.org/10.1002/cite.202100042.
[24] H. Chen, M. Zou, H. Dong, A.K. SenGupta, CO2-driven hybrid ion exchange: a resilient reverse osmosis pretreatment for high-recovery wastewater reuse, Water Res. 292 (2026) 125332, https://doi.org/10.1016/j.watres.2026.125332.
[25] J.C. Crittenden, R.R. Trussell, D.W. Hand, K.J. Howe, G. Tchobanoglous, MWH'S Water Treatment: Principles and Design, Third edition, John Wiley & Sons, Inc., Hoboken, New Jersey, 2012.
[26] M. Cornelsen, R. Weber, S. Panglisch, Minimizing the environmental impact of PFAS by using specialized coagulants for the treatment of PFAS polluted waters and for the decontamination of firefighting equipment, Emerg. Contam. 7 (2021) 63–76, https://doi.org/10.1016/j.emcon.2021.02.001.
[27] B. Thomson, K. Howe, C.O. Lee, The mineral recovery enhanced desalination (MRED) process for improved brackish water desalination, Water Reuse 14 (2024) 593–612, https://doi.org/10.2166/wrd.2024.058.
[28] P. McCleaf, W. Stefansson, L. Ahrens, Drinking water nanofiltration with concentrate foam fractionation—a novel approach for removal of per- and polyfluoroalkyl substances (PFAS), Water Res. 232 (2023) 119688, https://doi.org/10.1016/j.watres.2023.119688.
[29] Stadtwerke Duisburg: Chemisch - physikalische Wasseranalyse. 2025 9th of April 2026 Available from: https://www.stadtwerke-duisburg.de/fileadmin/user_upload/Veroeffentlichungen/Trinkwasseranalyse_Nord.pdf.
[30] M. Futterlieb, S. Panglisch, Early detection and control of $CaCO_3$ scaling in closed-circuit reverse osmosis under antiscalant-free conditions, Desalination 622 (2026) 119622, https://doi.org/10.1016/j.desal.2025.119622.
[31] M. Futterlieb, S. Panglisch, Incipient CaCO3-scaling detection for scaling mitigation, Desalination 613 (2025) 119023, https://doi.org/10.1016/j.desal.2025.119023.
[32] DuPont, FilmTec™ BW30 PRO-4040 & BW30 PRO-2540, 2024, 26th of September 2024]; Available from: https://www.dupont.com/content/dam/dupont/amer/us/en/water-solutions/public/documents/en/RO-FilmTec-BW30-PRO-4040-and-BW30-PRO-2540-PDS-45-D03970-en.pdf.
[33] P. Leube, M. Riedel, C. Vogel, Quantification of Perfluorocarboxylic Acids in Water Samples Via Static Headspace Gas Chromatography Coupled to Mass Spectrometry, in: SETAC Europe Vienna, 2025.
[34] E. Reid, Q. Ma, T. Igou, C.-H. Huang, Y. Chen, Insights on the adsorption of per- and Polyfluoroalkyl substances onto laboratory syringe membrane filters: experimental, materials, and mechanism evaluations, ACS ES&T, Water 6 (2026) 2047–2058, https://doi.org/10.1021/acsestwater.5c00438.
[35] K. Noda Morishita, H. Lee, C. Han, X.-Z. Niu, Syringe filters and autosampler vials impact on analysis of long-, short-, and ultrashort-chain per- and polyfluoroalkyl substances, ACS ES&T Water 5 (2025) 1344–1352, https://doi.org/10.1021/acsestwater.4c01090.
[36] DIC as Sum of Carbonate Species. 2026; Available from: https://www.aqion.de/site/90.
[37] T. Waly, M.D. Kennedy, G.-J. Witkamp, G. Amy, J.C. Schippers, The role of inorganic ions in the calcium carbonate scaling of seawater reverse osmosis systems, Desalination 284 (2012) 279–287, https://doi.org/10.1016/j.desal.2011.09.012.
[38] S. Lee, M. Elimelech, Relating organic fouling of reverse osmosis membranes to intermolecular adhesion forces, Environ. Sci. Technol. 40 (2006) 980–987, https://doi.org/10.1021/es051825h.
[39] C. Liu, X. Cheng, J. Bo, R. Gao, Y. Shen, Y. Zhi, D. Song, Q. He, Unraveling the synergistic impact of calcium ions and pH on the rejection of per- and perfluoroalkyl substances by nanofiltration in complex water matrices, J. Hazard. Mater. 501 (2026) 140666, https://doi.org/10.1016/j.jhazmat.2025.140666.
[40] S. Panglisch, M. Futterlieb, Membranverfahren - Grundlagen und Praxisanwendung, in: R. Winzenbacher, S. Panglisch (Eds.), Wasseraufbereitung - Grundlagen und Verfahren, Vulkan Verlag, 2025.
[41] A.E. Childress, M. Elimelech, Effect of solution chemistry on the surface charge of polymeric reverse osmosis and nanofiltration membranes, J. Membr. Sci. 119 (1996) 253–268, https://doi.org/10.1016/0376-7388(96)00127-5.
[42] E.M. Kimani, M. Pranić, S. Porada, A.J.B. Kemperman, I.I. Ryzhkov, W.G.J. van der Meer, P.M. Biesheuvel, The influence of feedwater pH on membrane charge ionization and ion rejection by reverse osmosis: an experimental and theoretical study, J. Membr. Sci. 660 (2022) 120800, https://doi.org/10.1016/j.memsci.2022.120800.
[43] X. Lv, Y. Sun, R. Ji, B. Gao, J. Wu, Q. Lu, H. Jiang, Physicochemical factors controlling the retention and transport of perfluorooctanoic acid (PFOA) in saturated sand and limestone porous media, Water Res. 141 (2018) 251–258, https://doi.org/10.1016/j.watres.2018.05.020.
[44] Y. Zhao, X. Min, S. Xu, Y. Wang, Adsorption of per- and Polyfluoroalkyl substances (PFAS) by aquifer materials: the important role of dolomite, Environ. Sci. Technol. Lett. 10 (2023) 931–936, https://doi.org/10.1021/acs.estlett.3c00583.
[45] J.G. Wijmans, R.W. Baker, The solution-diffusion model: a review, J. Membr. Sci. 107 (1995) 1–21, https://doi.org/10.1016/0376-7388(95)00102-I.
[46] E. Hosseinipour, E. Harris, H.A. El Nazer, Y.M.A. Mohamed, P.A. Davies, Desalination by batch reverse osmosis (RO) of brackish groundwater containing sparingly soluble salts, Desalination 566 (2023), https://doi.org/10.1016/j.desal.2023.116875.
[47] M. Li, Cyclic simulation and energy assessment of closed-circuit RO (CCRO) of brackish water, Desalination 545 (2023) 116149, https://doi.org/10.1016/j.desal.2022.116149.
[48] F.d. Dardel, Regeneration methods for ion exchange units, 24th of April 2026]; Available from: https://dardel.info/IX/processes/regeneration.html, 2026.
[49] W.H. Höll, K. Hagen, Partial demineralisation of drinking water using carbon dioxide regenerated ion exchangers, Water Supply 2 (2002) 57–62, https://doi.org/10.2166/ws.2002.0007.
[50] M. Park, K.D. Daniels, S. Wu, A.D. Ziska, S.A. Snyder, Magnetic ion-exchange (MIEX) resin for perfluorinated alkylsubstance (PFAS) removal in groundwater: roles of atomic charges for adsorption, Water Res. 181 (2020) 115897, https://doi.org/10.1016/j.watres.2020.115897.
[51] S.J. Chow, H.C. Croll, N. Ojeda, J. Klamerus, R. Capelle, J. Oppenheimer, J. G. Jacangelo, K.J. Schwab, C. Prasse, Comparative investigation of PFAS adsorption onto activated carbon and anion exchange resins during long-term operation of a pilot treatment plant, Water Res. 226 (2022) 119198, https://doi.org/10.1016/j.watres.2022.119198.
[52] B. Liu, Y.-L. Liu, M. Sun, Remove legacy perfluoroalkyl acids and emerging per- and polyfluoroalkyl ether acids by single-use and regenerable anion exchange resins: rapid small-scale column tests and model fits, Water Res. 257 (2024) 121661, https://doi.org/10.1016/j.watres.2024.121661.
[53] G. Abulikemu, J.G. Pressman, D.G. Wahman, G.A. Sorial, T.T. Sanan, E.K. Stebel, B. N. Gray, E.W. Hughes, E.J. Kleiner, S.G. Pedigo, C.X. Gastaldo, S.J. Smith, L. M. Haupert, J.B. Burkhardt, Perfluoroalkyl chemical adsorption by granular activated carbon: impacts of source water characteristics, AWWA Water Sci. 7 (2025) e70027, https://doi.org/10.1002/aws2.70027.
[54] G. Kim, D.N. Mengesha, Y. Choi, Adsorption dynamics of per- and polyfluoroalkyl substances (PFAS) on activated carbon: interplay of surface chemistry and PFAS structural properties, Sep. Purif. Technol. 349 (2024) 127851, https://doi.org/10.1016/j.seppur.2024.127851.
[55] M. Riegel, B. Haist-Gulde, F. Sacher, Sorptive removal of short-chain perfluoroalkyl substances (PFAS) during drinking water treatment using activated carbon and anion exchanger, Environ. Sci. Eur. 35 (2023) 12, https://doi.org/10.1186/s12302-023-00716-5.
[56] Y. Matsui, Y. Fukuda, T. Inoue, T. Matsushita, Effect of natural organic matter on powdered activated carbon adsorption of trace contaminants: characteristics and mechanism of competitive adsorption, Water Res. 37 (2003) 4413–4424, https://doi.org/10.1016/S0043-1354(03)00423-8.
[57] B. Haist-Gulde, Adsoprtion an Aktivkohle, in: S. Panglisch, R. Winzenbacher (Eds.), Wasseraufbereitung - Grundlagen und Verfahren, Vulkan Verlag, 2025.